Icarus 265 (2016) 187–208

Contents lists available at ScienceDirect

Icarus

journal homepage: www.journals.elsevier.com/icarus

The early geodynamic evolution of Mars-type planets

Siqi Zhang *, Craig O'Neill

Macquarie Planetary Research Centre and ARC Centre of Excellence for Core to Crust Fluid Systems/GEMOC, Department of Earth and Planetary Science, Macquarie University, NSW 2019, Australia

ARTICLE INFO

Article history:
Received 5 June 2015
Revised 18 October 2015
Accepted 21 October 2015
Available online 24 October 2015

Keywords:
Geophysics
Mars
Planetary dynamics
Thermal histories

ABSTRACT

It is not clear whether Mars once possessed active tectonics, yet the question is critical for understanding the thermal evolution of Mars, and the origin and longevity of its early dynamo. To address these issues, we have coupled mantle flow simulations, together with parameterized core evolution models, to simulate the early evolution of Mars-like planets, and constrain the influence of early mobile-lid tectonics on core evolution. We have explored a wide parameter suite, encapsulating a range of uncertainties in initial conditions, rheological parameters, and surface strength. We present successful models that experience early mobile-lid behaviour, with a later transition into a stagnant-lid mode, which reproduce core dynamo histories similar to the magnetic history of early Mars.

1. Introduction

The early geological history of Mars exhibits evidence of high (~1 bar) atmospheric pressures, flowing water, and voluminous volcanism (e.g. Baker et al., 1991). It is unclear, however, if Mars ever possessed active tectonics.

One of the major outstanding problems in simulating martian evolution is the formation of the hemispheric dichotomy. Two broad scenarios exist; that the dichotomy was created by exogenic processes, such as a giant impact (Wilhelms and Squyres, 1984; Andrews-Hanna et al., 2008) or several large impacts (Frey and Schultz, 1988; Head, 2002), or that it was formed by endogenic processes, due to internal, degree-one convection features (e.g. Zhong and Zuber, 2001; Roberts and Zhong, 2006). For example, the low topography, thin crust, smooth surface, and young apparent age of the Northern Lowlands – which cover ~40% of the planet – have been suggested to be caused by seafloor spreading (Sleep, 1994). However, the suggestion of crypto-craters beneath the volcanic surface lithology hints at an older, non-plate tectonic origin, and the basin morphology has been suggested to be consistent with a giant impact (Andrews-Hanna et al., 2008). An alternative to impacts are endogenous processes; either plate tectonics, an early post-magma ocean overturn event (Debaille et al., 2009; Tosi et al., 2013), or degree-one plume activity (Roberts and Zhong, 2006). A problem with the latter scenario is that early Mars mantle was likely to be hot and vigorously convecting, and such conditions do not favour degree one convection. In order to obtain degree one patterns, Zhong and Zuber (2001) and Roberts and Zhong (2006) employed a strongly stratified mantle viscosity. An alternative is the effect of the perovskite phase change, which occurs near the core mantle boundary on Mars (Harder and Christensen, 1996; Breuer et al., 1998).

A more challenging question, perhaps related to dichotomy formation, is the formation of the Tharsis Rise, which is near the dichotomy boundary. Kiefer (2003) demonstrated that the post-Noachian evolution of Tharsis can be explained by the impingement of a long-lived mantle-upwelling under the province. Van Thienen et al. (2006) offered an explanation invoking active tectonics in the northern hemisphere. Zhong (2009) and Šrámek and Zhong (2010) suggested a stagnant-lid degree one plume formed underneath a thick lithosphere keel, which resulted in a rotation of the lithospheric shell, bringing the Tharsis plume to the boundary of the dichotomy.

The identification of magnetic lineations in the Southern Highlands (Acuna et al., 1999) led to the suggestion that this region of thickened crust formed via a process analogous to seafloor spreading – albeit at hotter mantle temperatures (hence the thickened crust). The width of these lineations (on the order of 100 km) is also markedly different to Earth (on the order of 10 km) (Connerney et al., 1999), suggesting either different rates of spreading, or of magnetic reversals.

Indeed, the existence of an early (4.5–4.0 Ga) magnetic field on Mars (Acuna et al., 1999) has been suggested to be a consequence of plate tectonic-like processes. Vigorous convection in the core is required to drive an active geodynamo, which occurs if there is a large heat flux (>19 mW/m^2) out of the core–mantle boundary (Nimmo and Stevenson, 2000). This condition may not be met for

* Corresponding author.
E-mail address: siqi.zhang@mq.edu.au (S. Zhang).

http://dx.doi.org/10.1016/j.icarus.2015.10.019
0019-1035/

Table 1
Key model parameters.

Mars radius	R	3385 km
Core radius	R_c	1700 km
Gravity acceleration	G	3.7 m/s^2
Initial CMB temperature	T_{CMB}	2210 K
Thermal conductivity	k	4.7 W/mK
Pre-exponent factor	A	3.0×10^{15} Pa s
Activation energy	E	157 kJ/mol
Activation volume	V	1.5 cm^3/mol
Reference viscosity (at 1600 K, 0 GPa)	η_0	4.0×10^{20} Pa s
Surface yield stress	$\sigma_{surface}$	1.0 MPa
Friction coefficient	f	0.08

Table 2
Heating rate, half-life and present-day concentration of radioactive isotopes.

Isotope	Heating rate H (W/kg)	Half-life (year)	Concentrations (ppm)
U			0.016
^{238}U	9.46×10^{-5}	4.47×10^9	0.01588
^{235}U	5.69×10^{-4}	7.04×10^8	0.00011
^{232}Th	2.64×10^{-5}	1.40×10^{10}	0.056
K			305
^{40}K	3.48×10^{-9}	1.25×10^9	0.03630

Table 3
Parameters for the core.

CMB pressure	P_c	20 GPa
Light element composition	X_0	10 wt%
Density at the centre of the core	ρ_c	7.3×10^3 kg/m^3
Core density at zero pressure	ρ_{c0}	6.5×10^3 kg/m^3
Core incompressibility at zero pressure	K_{c0}	3.0×10^{11} Pa
Core thermal expansion coefficient	α_c	5.85×10^{-5} K^{-1}
Core heat capacity	Cp_c	780 J/kg/K
Latent heat	L_h	750×10^3 J/kg
Core thermal conductivity	k_c	40 W/m/K
Light element partition factor	Δ	0.5
Parameters for core solidus	T_{m0}	1811 K
	T_{m1}	13.35×10^{-12} Pa^{-1}
	T_{m2}	-13.94×10^{-23} Pa^{-2}
	θ	2.41

The core parameters are from Williams and Nimmo (2004).

a stagnant planet – where the hot core sees a hot mantle directly above it – but may be met if cold subducted slabs can reach the core–mantle boundary. This constraint has been explored by e.g. Nimmo and Stevenson (2000), Breuer and Spohn (2003), Williams and Nimmo (2004), and O'Neill et al. (2007a), who found a hot early core may in fact develop a large enough heat flux, even for a stagnant planet, to power a geodynamo, if core–mantle boundary temperatures exceeded ~1850 °C. Furthermore, it is not clear whether Mars has a solid inner core or not (e.g. Stevenson, 2001), and a fully liquid core with high concentration of light-elements is possible (e.g. Schubert and Spohn, 1990).

A further constraint on heat flux comes from estimates of elastic lithospheric thickness for different martian terranes (McGovern, 2002, 2004). Younger Amazonian loading events (e.g. Olympus Mons, Pavonis Mons) exhibit thick elastic lithospheres, and lower estimated heat fluxes (on the order of ~13–28 mW/m^2). Hesperian heat fluxes range from ~11 to 40 mW/m^2, and those calculated for the Noachian (e.g. Hellas Basin, Noachis Terra, etc.) have heat fluxes in excess of >35–50 mW/m^2, depending on the terrane.

Crustal production is also an important constraint on the evolution of Mars. This has been more specifically addressed by parameterized models (e.g. Breuer and Spohn, 2003, 2006), and 2D/3D mantle convection simulations (e.g. Keller and Tackley, 2009; Ruedas et al., 2013; Sekhar and King, 2014). However, most of these evolutionary models consider the progression of a stagnant-lid regime on Mars. Even in models invoking mobile-lid tectonics (e.g. Nimmo and Stevenson, 2000), or hemispheric tectonic activity (e.g. Van Thienen et al., 2006), the physical plausibility of mobile-lid behaviour, and transition from mobile-lid to stagnant-lid under early martian conditions has rarely been carefully explored. An exception is Lenardic et al. (2004) who suggested mobile-lid tectonics was shut-off by growth of the Southern Highlands.

Lastly, recent work by Tuff et al. (2013) found the generally older (~3.7 Gyr) Gusev crater rocks are from a more oxidised magma source than the younger igneous SNC meteorites, which were sourced from greater depths. Mars became more oxidised by losing its early hydrogen to space, via sputtering and other atmospheric loss mechanisms, resulting in extremely oxidised surface rocks. In order for the magma source to become oxidised, it was inferred that this oxidised surface must, at some point, have been recycled into the mantle source of these magmas. This implies not only a surface recycling mechanism, but also constrains the timing of this mechanism via the timescale for atmospheric loss. The modelling studies suggests catastrophic atmosphere loss occurred during the first ~500 Myr of its early history (e.g. Lammer et al., 2012), and the martian surface likely became oxidised during this period. The surface recycling mechanism was likely operable some period after the surface was oxidised (>4.0 Ga), and prior to ~3.7 Ga when the Gusev crater rocks were formed.

In short, there are a number of lines of circumstantial evidence to suggest that Mars did once have some form of surface tectonics, or tectonic episodes. However most previous modelling of martian tectonics has focused on stagnant-lid convection. The aim of this paper is to constrain the physical plausibility of tectonics on an evolving Mars-type planet, and understand the specific predictions and implications of this style of evolution. To do this, we use 2D and 3D mantle convection simulations in a spherical geometry using the code ASPECT (Kronbichler et al., 2012). Importantly, we consider the evolution of the planet from its post-magma ocean thermal state, with evolving heat production, and basal core temperatures. We track the evolution of melting, and couple the model with a parameterized model of core evolution to constrain the implications of these models for magnetic field evolution.

2. Numerical method

The model is built upon the open source finite element code ASPECT (http://aspect.dealii.org/). The mantle is treated as a compressible Stokes fluid, and compositional fields are included to help track the migration of different materials. The conservation equations of mass, momentum, energy, as well as that of compositional fields, are given by the following:

$$\nabla \cdot (\rho \vec{u}) = 0 \tag{1}$$

$$-\nabla \cdot \left[2\eta\left(\boldsymbol{\varepsilon}(\vec{u}) - \frac{1}{3}(\nabla \cdot \vec{u})\boldsymbol{I}\right)\right] + \nabla p = \rho \vec{g} \tag{2}$$

$$\rho C_p\left(\frac{\partial T}{\partial t} + \vec{u} \cdot \nabla T\right) - \nabla \cdot k \nabla T = \rho H + \alpha T(\vec{u} \cdot \nabla p) + 2\eta\left(\dot{\boldsymbol{\varepsilon}}(\vec{u}) - \frac{1}{3}(\nabla \cdot \vec{u})\boldsymbol{I}\right) : \left(\dot{\boldsymbol{\varepsilon}}(\vec{u}) - \frac{1}{3}(\nabla \cdot \vec{u})\boldsymbol{I}\right) \tag{3}$$

$$\frac{\partial c_i}{\partial t} + \vec{u} \cdot \nabla c_i = 0 \tag{4}$$

where $\vec{u}$ is velocity, p is pressure, T is temperature, c_i is a compositional field (used to represent crust in one of our models in particular), ρ is the density, η is the viscosity, k is the heat conductivity, H is the internal heating rate, α is the thermal expansivity, g is the gravity acceleration, $\boldsymbol{I}$ is identity matrix, and $\dot{\boldsymbol{\varepsilon}}(\vec{u}) = \frac{1}{2}(\nabla\vec{u} + \nabla\vec{u}^T)$ is the strain rate tensor. The energy equation incorporates internal heating, viscous heating and adiabatic heating. The spinel-perovskite structure phase change is likely to occur near the core–mantle boundary for Mars-type planets. While some studies suggest that this phase change will suppress the smaller plumes, and help to establish degree-one martian convection (e.g. Harder and Christensen, 1996; Breuer et al., 1998), the main focus of this research is to test the plausibility of early mobile-lid tectonics, and for simplicity latent heat and viscosity changes related to possible phase changes are not included in our model.

For the discretization, a second order element is used for temperature and velocity, but first order elements for the pressure to satisfy LBB (Ladyzhenskay–Babuska–Brezzi) conditions. The energy and Stokes equations are solved only once each time step using an IMPES (Implicit Pressure, Explicit Saturation) time stepping scheme. In the energy equation, BDF-2 (Backward Differentiation Formula scheme of order 2) time stepping is used to replace the time derivative. The time step is automatically adjusted to fit CFL (Courant–Friedriches–Lewy) conditions. Instead of a fully compressible formulation, the compressibility has been simplified as vertically compressible (i.e. the compressibility is treated as dependant on static pressure only) to keep the Stokes equations symmetric. Readers can refer to the ASPECT manual for more details on numerical treatments (http://aspect.dealii.org/). At the surface boundary, free-slip is used for the Stokes equations and the temperature is fixed. At the bottom boundary, a fixed boundary is used for the Stokes equations, and the temperature is dynamically adjusted using a core evolution model detailed in the following sections. And no-flux boundary condition is used for all compositional fields. The computational mesh is refined at boundary layers, so the highest grid resolution on surface is around 14 km in 2D models and 56 km in 3D models, however the velocity and temperature use second order elements, so the effective resolution is in fact doubled to 7 km in 2D, and 28 km in 3D, if compared to results using lower order elements.

2.1. Visco-plastic rheology

The composition and rheological parameters for Mars are likely similar to Earth's upper mantle. However our understanding of the rheology is limited by experimental conditions. Most of the experiments are done under low pressures, and all experiments are carried out under much larger strain rates than occur naturally (10^{-4}–10^{-6} s^{-1} in laboratory compared to 10^{-9}–10^{-13} s^{-1} in natural shear zones) – meaning the results have to be extrapolated into real geodynamical conditions. This results in large uncertainties in our rheological parameters (e.g. reviewed by Bürgmann and Dresen, 2008; Karato, 2010). For simplicity here we use visco-plastic rheology, with an Arrhenius type viscosity law to account for diffusion creep, accompanied with a Byerlee type surface yielding.

2.1.1. Arrhenius rheology

We adopt a simplified Arrhenius viscosity of the form:

$$\eta(p,T) = Ae^{\frac{E+pV}{RT}} \tag{5}$$

where p is the pressure, T is the temperature, R is the gas constant, E is the activation energy, V is the activation volume, and the A is the pre-exponent factor. We have not considered strain-rate, or grain size, dependence explicitly. In this Newtonian formation, the activation energy E is implicitly divided by the stress exponent n (e.g. Christensen, 1983) – though non-Newtonian behaviour is introduced by plastic yielding, described below.

Although present-day Mars lacks significant liquid water on surface, early Mars' surface may have been water/ice rich, as suggested by atmospheric composition, surface geology, and the study of SNC meteorites as summarized by Carr (1987). As a result, we assume a wet rheology on early Mars. As the pressure in the martian mantle is much smaller than for Earth at similar depths, the rheology of the whole martian mantle is more akin to the upper

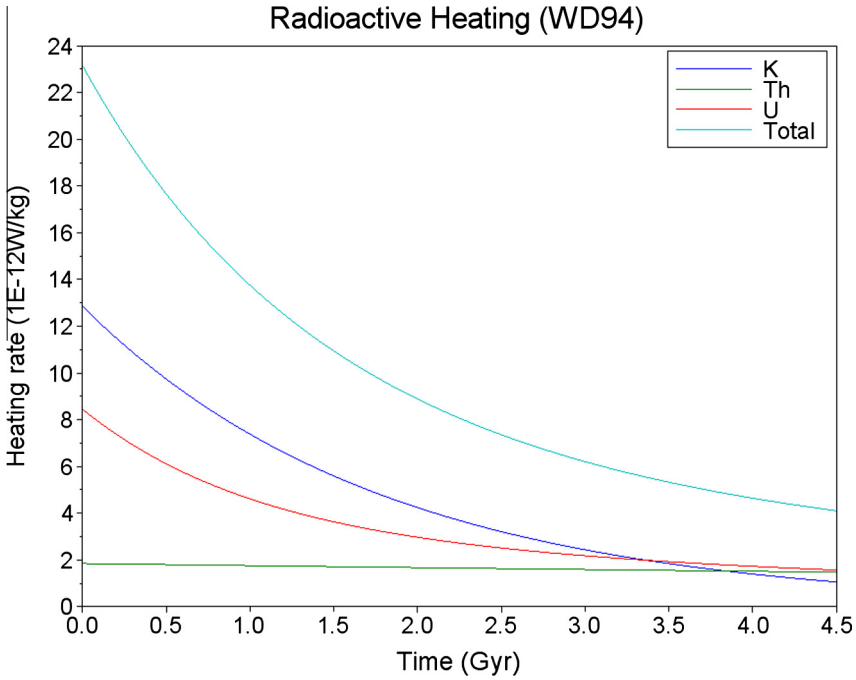

Fig. 1. Martian radioactive heating decaying through time, based on the heating rates in Table 2.

Fig. 2. Evolution of mobile-lid convection (labelled '**Ref**') vs. a stagnant-lid model (labelled '**Stag1**'), and a stagnant-lid model with a 200 K hotter core (labelled '**Stag2**'). The Ref model uses the reference parameters in Table 1. The **Stag1**/**Stag2** model has same except a surface yield stress of 50 MPa, and convection ubiquitously falls into a stagnant regime.

mantle of the Earth, i.e. dislocation creep dominating in the upper part, while diffusion creep is likely to play a more important role in the lowermost martian mantle.

However, the values of the rheological parameters in Eq. (5) under high pressures is still debated (e.g. reviewed by Bürgmann and Dresen, 2008), due to a lack of experiments at relevant pressures and relevant strain-rates – this is especially a problem for the activation volume. Previous models have utilised a wide range of activation energies, for similar Arrhenius formulations. While high values of ~300 kJ/mol, based on the diffusion creep of dry olivine (e.g. Karato and Wu, 1993), have been used by some workers (e.g. Breuer and Spohn, 2006; Van Thienen et al., 2006), lower values are also used in many studies (e.g. 120 kJ/mol by Zhong and Zuber (2001); 157 kJ/mol by Roberts and Zhong (2006), Šrámek and Zhong (2010), Sekhar and King (2014); 200 kJ/mol by Keller and Tackley (2009)). Although not explicitly mentioned within most of those papers, the difference in activation energies used is generally due to the dislocation creep activation energy being divided by the stress exponent n, when using a simplified Newtonian viscosity law such as Eq. (5), in order to produce an equivalent temperature dependence (Christensen, 1983). This also affects the activation volume. As a result, we adopt a low reference activation energy of 157 kJ/mol, following Roberts and Zhong (2006), and a small reference activation volume of 1.5 cm^3/mol. We explore different values of activation energy and volume in different models, as discussed in the later sections.

2.1.2. Plastic yielding

As mentioned above early Mars was likely to have a water rich surface – this results in a much lower surface yield stress, which may be close to the value of present-day Earth.

In our model, we included a Byerlee law type pressure dependent yield stress of the form:

$$\sigma_{yield} = \sigma_{surface} + fP \tag{6}$$

where $\sigma_{surface}$ is the yield stress at surface, f is the friction coefficient, and P is the pressure. Here we choose a small surface yield stress (1 MPa), and explore different friction coefficients from 0.08 to 0.15. Those parameters are comparable to previous work on mobile-lid tectonics (e.g. Moresi and Solomatov, 1998; Di

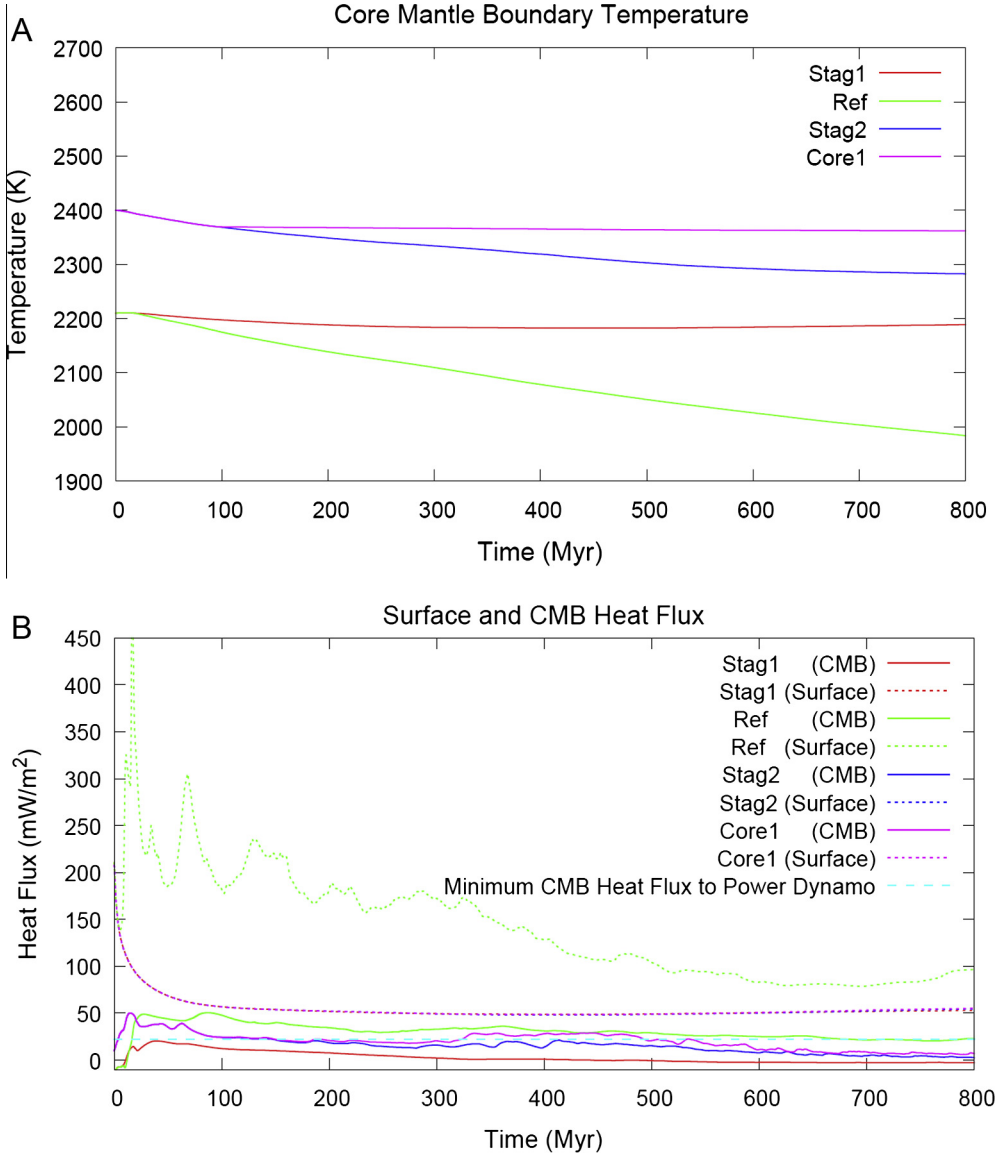

Fig. 3. Evolution of core–mantle temperature (A), heat flux (B), excess entropy (C), and melt production (D) for mobile-lid (**Ref**), stagnant-lid (**Stag1**), stagnant-lid with a hotter core (**Stag2**), stagnant-lid with hotter core and inner core growth (**Core1**).

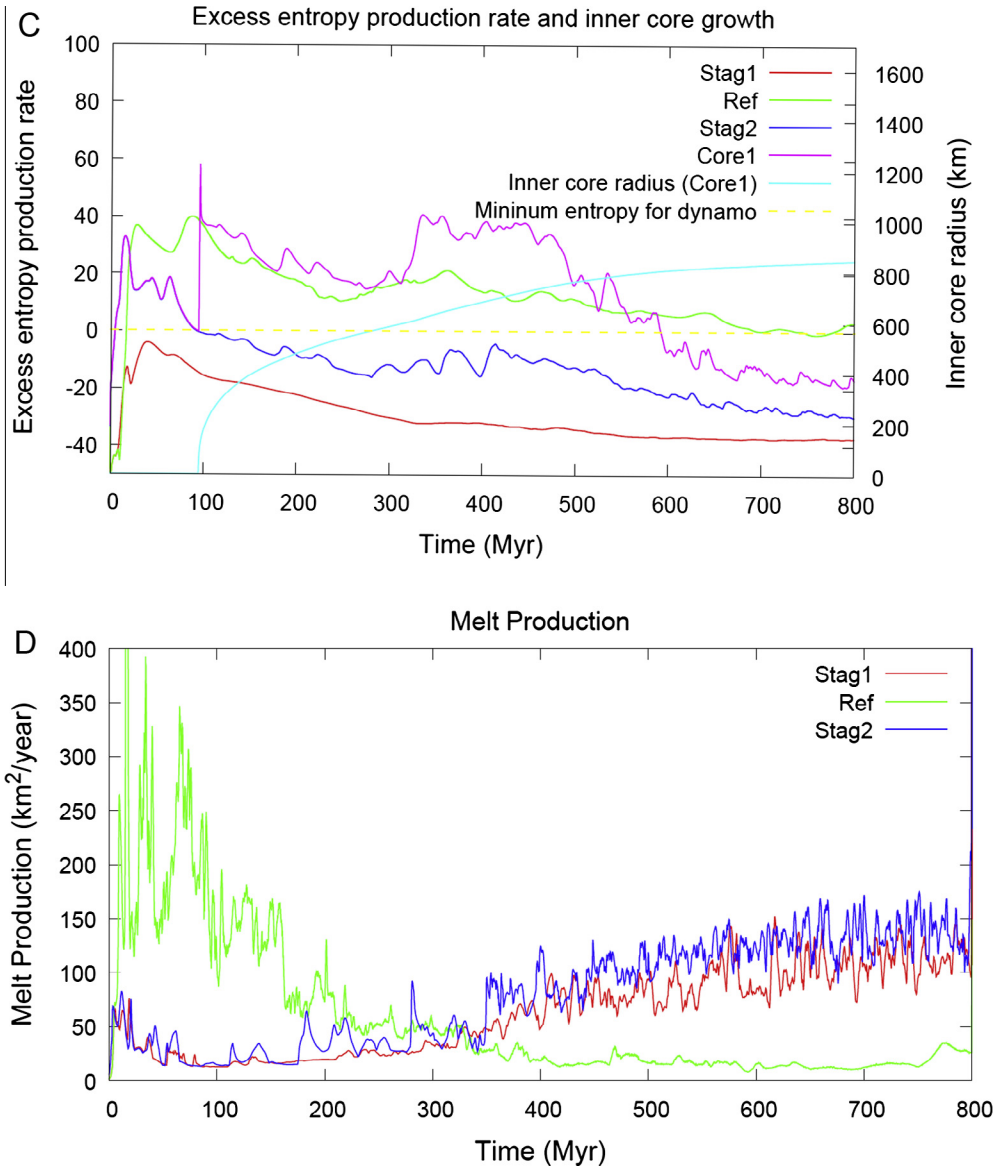

Fig. 3 (*continued*)

Giuseppe et al., 2008; O'Neill et al., 2009; Stadler et al., 2010), and are close to laboratory values for brittle deformation for water-altered rheologies (e.g. Escartin et al., 2001).

The effective viscosity η_e is limited by the yield stress in the following form:

$$\eta_e = min\left(\eta, \frac{\sigma_{yield}}{2\dot{\varepsilon}_{II}}\right) \tag{7}$$

where $\dot{\varepsilon}_{II}$ is the second invariant of the strain rate tensor.

2.1.3. Viscosity cut-off

An Arrhenius type rheology will result in very large viscosity contrasts in the lithosphere. Although extreme viscosities may be limited with suitable surface yielding, large viscosity contrasts will result in convergence problems for numerical codes. As a result, we apply viscosity cut-offs beyond 3×10^{23} Pa s, and $\sim 5 \times 10^{19}$ Pa s. However it incorporates the range relevant to geodynamic processes, and is still able to reproduce the physics of the problem. The top cut-off is chosen, together with a lithosphere yielding parameter, which not only allows surface yielding but also allow other forms of deformation processes to take place. The bottom cut-off value is chosen to incorporate most observed mantle viscosity values.

Previous work using a Frank-Kamenetskii rheology suggest that the convection regime may shift from mobile-lid to stagnant-lid as a result of an increase in the viscosity contrast from 10^4 to 10^5 (e.g. Moresi and Solomatov, 1995). Arrhenius type viscosities give much sharper viscosity contrasts at the bottom of the lithosphere, which reduces the lithospheric stress. As a result we do not observe these regime shifts for the viscosity cut-offs used. However, higher cut-offs primarily result in high viscosity gradients within the very top brittle portion of the lithosphere, resulting in difficulty converging with yielding in place.

2.2. Mineral physics parameters

The mineral physics parameters such as density, heat capacity, thermal expansivity, and compressibility are assumed to be pressure and temperature dependent and calculated from a lookup table generated by Perplex (http://www.perplex.ethz.ch/). This

table uses a thermo-dynamic database by Stixrude and Lithgow-Bertelloni (2011) and assumes a pyrolitic composition of Ringwood and Irifune (1988). Thermal conductivity is assumed to be constant in this study. The key parameters for the reference model are listed in Table 1.

2.3. Radioactive heating

In many mantle convection studies, the internal heating rate is taken to be constant. However it may not be suitable for modelling the evolution of a planet for longer periods, especially when considering the early history of a planet, during which the decay of internal heating rate is rapid, and may become a crucial factor in determining mantle dynamics. In this study, we use a time dependent model for internal heating rate by following Turcotte and Schubert (2002), where the concentration of radioactive elements K, Th, U is taken from martian meteorite studies by Wanke et al. (1994). The present day concentration of ^{238}U and ^{235}U are assumed to be 99.28 wt% and 0.71 wt% of natural uranium, ^{232}Th is 100 wt% of natural thorium, and ^{40}K is 0.0119 wt% of natural potassium, as shown in Table 2. The decay of radioactive heating rate is shown in Fig. 1. We do not consider extremely short-lived isotopes such as ^{26}Al, or ^{60}Fe, as they contribute primarily in determining the initial condition for these models. However, the uncertainty of internal heating rates for early Mars is still very large; Lodders and Fegley (1997) provide different concentrations with much higher concentrations of potassium which lead to significantly larger internal heating rates in early martian history. In addition, the partition coefficient of radioactive elements between crust and mantle is not well defined, and it may also evolve over time due to extraction of HPEs by magmatism (e.g. O'Neill et al., 2005). The comparison of different internal heating models and the partition process of HPEs between the mantle and crust has been investigated in several other studies (e.g. O'Neill et al., 2005; Ogawa and Yanagisawa, 2011; Ruedas et al., 2013; Sekhar and King, 2014). As a result we don't explore this topic in detail in this study, and assume the radioactive elements are uniformly distributed within mantle and crust for simplicity.

2.4. Core evolution

The core mantle boundary temperature is treated as a constant in many mantle convection studies. When the viscosity is strongly temperature dependent, however, changes in core–mantle temperature not only affect the mantle temperature contrast that drives the convection, but also lead to significant changes in mantle viscosity, that strongly influence the mantle dynamics. For models of the early evolution of planets in which the core cooling rate is assumed to be very high, or for models focused on planetary evolution over extended periods, the effect of evolving core–mantle boundary temperatures cannot be ignored. Some previous studies have addressed this issue by using a predefined core mantle temperature drop (e.g. O'Neill and Debaille, 2014; Sekhar and King, 2014), though only a few have used dynamically evolving core mantle boundary temperature (e.g. Ke and Solomatov, 2009; Ruedas et al., 2013). In our study, we included a more practical core evolution model in our mantle flow simulations to understand the coupling between mantle dynamics and core evolution. A parameterized core formulation considering a one-dimensional core model which includes energy and entropy balances has been used, following from Nimmo et al. (2004).

The density, gravity, adiabatic temperature, and pressure in the core are dependent on each other, and it is difficult to solve this coupled system. One approach is to parameterize profiles of these properties into a third order polynomial form of radius, as per Labrosse et al. (2001). Here we assume density, gravity, adiabatic temperature, and pressure vary with radius, and are parameterized by ignoring high order terms in the following form:

$$\rho(r) = \rho_c \exp\left(-\frac{r^2}{L^2}\right) \tag{8}$$

$$g(r) = \frac{4\pi}{3} G\rho_c r\left(1 - \frac{3r^2}{5L^2}\right) \tag{9}$$

$$T_a(r) = T_{\mathrm{CMB}} \exp\left(\frac{R_c^2 - r^2}{D^2}\right) \tag{10}$$

$$P(r) = P_c + \frac{4\pi G\rho_c^2}{3}\left[\left(\frac{3r^2}{10} - \frac{L^2}{5}\right)\exp\left(-\frac{r^2}{L^2}\right)\right]_r^R \tag{11}$$

where $L = \sqrt{\frac{3K_{c0}\left(\log\frac{\rho_c}{\rho_{c0}}+1\right)}{2\pi G\rho_{c0}\rho_c}}$ and $D = \sqrt{\frac{3C_{P_c}}{2\pi\alpha_c\rho_c G}}$ are length scale parameters, and K_{c0} and ρ_{c0} are the density and compressibility of the core at zero pressure.

The energy and entropy balance are calculated using the following equations:

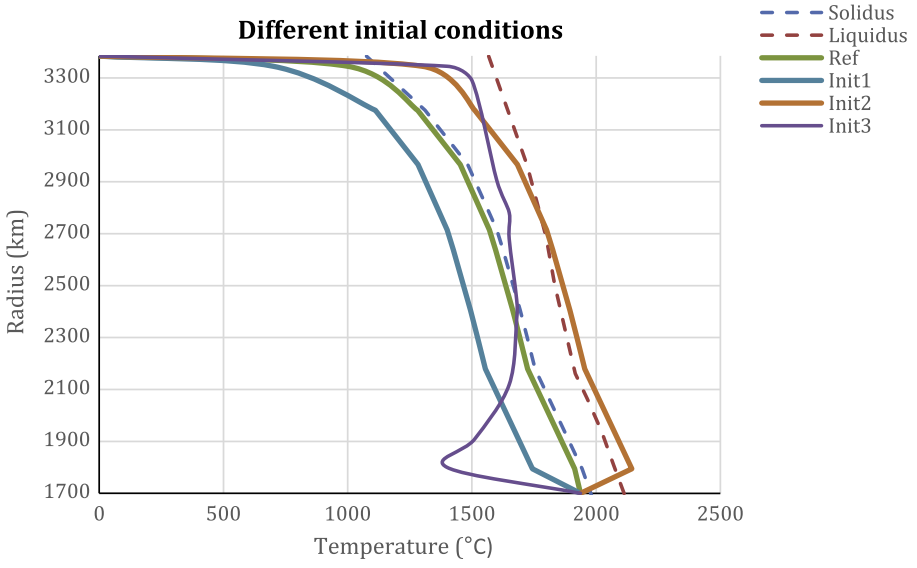

Fig. 4. Different initial temperature profiles. Mantle solidus and liquidus are given by Longhi et al. (1992).

Fig. 5. The model evolution of different initial conditions: 1. **Init1** cooler model which is 200 K cooler than the reference model **Ref**; 2. **Init2** hotter model, which is 200 K hotter than reference model; 3. **Init3** over turned solidus.

$$Q_R - Q_c = (Q_L + Q_G)\frac{\partial R_i}{\partial t} + Q_s\frac{\partial T_{\mathrm{CMB}}}{\partial t} \tag{12}$$

$$\Delta E = E_R + E_s\frac{\partial T_{\mathrm{CMB}}}{\partial t} + (E_L + E_G)\frac{\partial R_i}{\partial t} - E_k \tag{13}$$

Here Q_R is radioactive heating, $Q_s \frac{\partial T_{\mathrm{CMB}}}{\partial t}$ is the specific heat term, $Q_L \frac{\partial R_i}{\partial t}$ the latent heat term, $Q_G \frac{\partial R_i}{\partial t}$ is the gravitational contribution from inner core growth, and Q_c is the heat flow through the CMB. The subscripts denote the same contributions in the entropy equation, and E_k is the entropy caused by the heat flow through the core adiabat. The specific heat term in both equations is dependent on the rate of change of the core mantle boundary temperature $\frac{\partial T_{\mathrm{CMB}}}{\partial t}$, and the latent heat and gravitational contribution depends on the rate

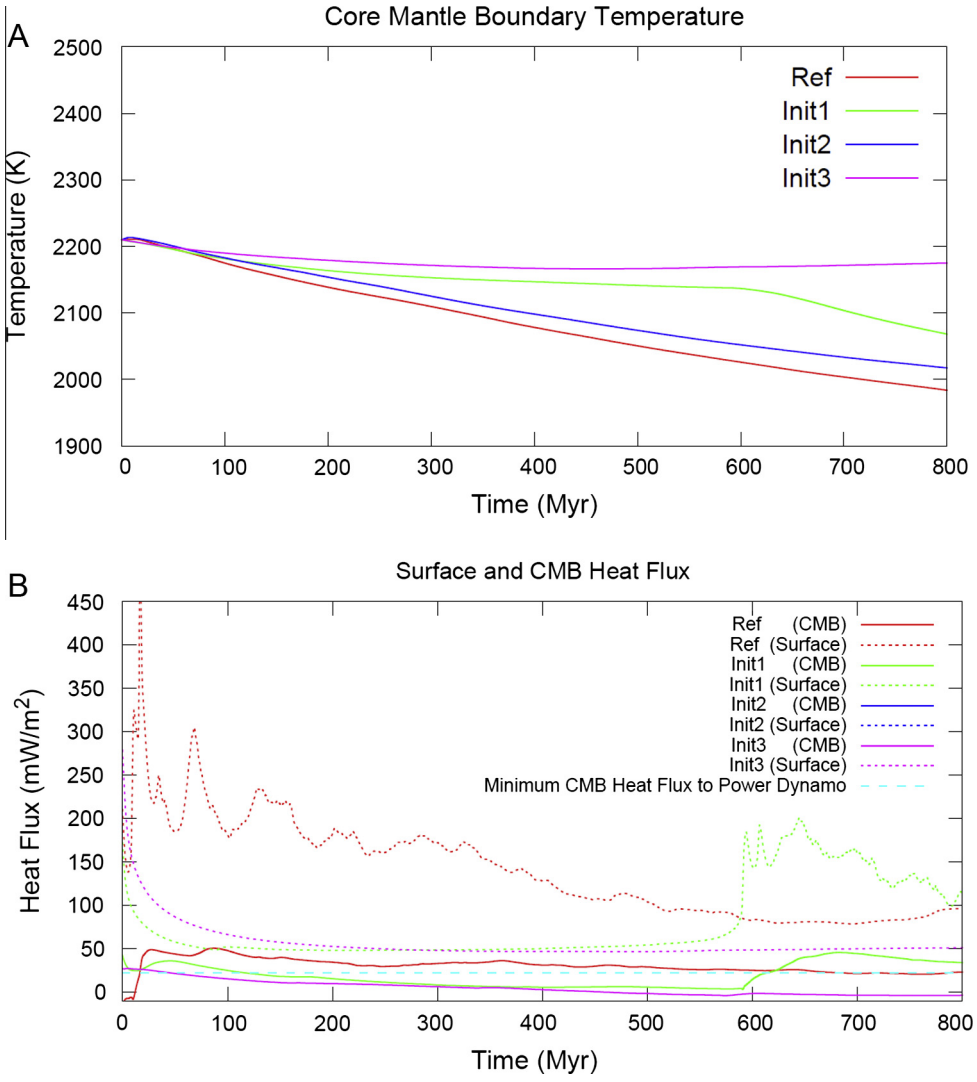

Fig. 6. Evolution of core–mantle temperature (A) and heat flux (B) for different initial conditions (**Init1**/**Ref**/**Init2**/**Init3**).

of growth of the inner core $\frac{\partial R_i}{\partial t}$, which will vanish when the core is completely liquid or completely frozen. Detailed formulations of each term can be found in Nimmo et al. (2004), Gubbins et al. (2003), and Gubbins et al. (2004).

The core solidus can be parameterized as (Schubert et al., 1988):

$$T_m(p) = T_{m0}(1 - \theta\chi)(1 + T_{m1}p + T_{m2}p^2) \tag{14}$$

where χ is the mass fraction of light element S, and θ is the Fe melting depression factor by S.

While Schubert et al. (1988) assumed light elements will be completely excluded from the inner core during the solidification, we follow Nimmo et al. (2004)'s approach that light elements are excluded by a partition factor Δ using the following equation:

$$\chi = \frac{\chi_0}{(1 - \xi^3) + \Delta\xi^3} \tag{15}$$

where the initial concentration is χ_0, and $\xi = \frac{R_i}{R}$ is the radius ratio between the inner core and the whole core.

Finding the intersection point of the core solidus and core adiabatic can give the pressure at inner–outer core boundary, which can be used to determine the inner core radius using Eq. (11).

So as the core mantle boundary heat flow Q_c is given by the mantle flow simulation for different time steps, the relationship between inner core radius R_i, light element concentration in the outer core χ, and the core mantle boundary temperature T_{CMB} is in the following form:

$$T_{CMB} = T_{CMB}\left(Q_c, \frac{\partial R_i}{\partial t}\right) \tag{16}$$

$$R_i = R_i(T_{CMB}, \chi) \tag{17}$$

$$\chi = \chi(R_i) \tag{18}$$

Solving this system with explicit iteration through each time step is difficult and will have strong instability issues. Instead of solving T_{CMB} and R_i to match the above system, we consider the relative proportions of energy from core cooling (related to $\frac{\partial T_{CMB}}{\partial t}$) and inner core growth (related to $\frac{\partial R_i}{\partial t}$). After introducing a new coefficient a in the core energy balance equation that defines the energy ratio of core cooling in the total core energy change rate (i.e. the ratio of heating rate to the heat flow through CMB), the changing core–mantle temperature and inner core radius through time can be separated, then the core energy balance equation becomes:

$$(1 - a)(Q_R - Q_c) = (Q_L + Q_G)\frac{\partial R_i}{\partial t} \tag{19}$$

$$a(Q_R - Q_c) = Q_s\frac{\partial T_{CMB}}{\partial t} \tag{20}$$

Fig. 7. Model evolution for different friction coefficients. The reference model **Ref** has a surface yield stress of 1 MPa, and a friction coefficient of 0.08. Models **Fric1**/**Fric2**/**Fric3** have friction coefficients of 0.10/0.12/0.15 respectively.

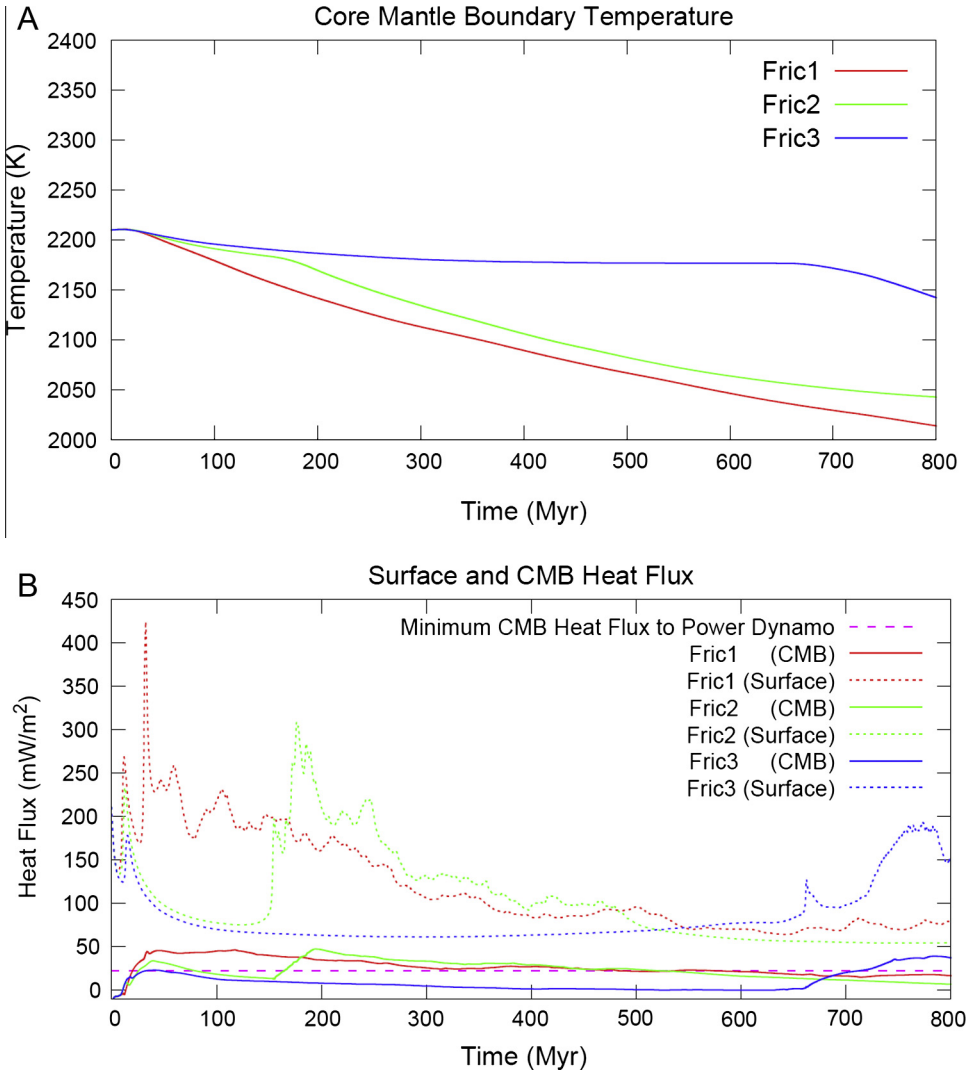

Fig. 8. Evolution of core–mantle temperature (A), and heat flux (B) for different lithosphere yielding criteria (**Fric1**/**Fric2**/**Fric3**).

For any given a between 0 and 1 a new T_{CMB} and R_i can be calculated in each time step. T_{CMB} and R_i are constrained in that the core solidus and adiabatic profile converge at the R_i. The problem becomes to find a suitable coefficient a between 0 and 1 that fits this constraint. As this problem has a single solution while the inner core is growing, this can be easily solved with a bisection method.

Whether Mars currently has a solid inner core, or a fully molten core due to a high concentration of light elements (mainly S), is unclear. However, martian core evolution models do not favour low S content, as inner core growth models result in a long-lasting dynamo, from the addition of energy from compositional convection (e.g. Williams and Nimmo, 2004). Similar behaviour also can be found in core evolution models for the Earth, once the inner core starts to grow (e.g. Gubbins et al., 2004; Nimmo et al., 2004). Furthermore, laboratory studies of iron–sulphur and iron–nickel–sulphur systems under martian core conditions also support a fully molten core (e.g. Stewart et al., 2007). As a result, we choose a high core sulphur content (of 10 wt%) which does not result in a solid inner core throughout the timescale of our simulations. We also test one model to explore the effects of the inner core growth. The parameters for the core evolution are listed in Table 3.

2.5. Initial conditions

The initial conditions for planetary evolution models, as explored here, are the most challenging part of the problem. During planetary formation and core mantle segregation, a magma ocean is purported to have formed (e.g. Elkins-Tanton, 2005). The magma ocean is believed to freeze fast due to vigorous convection (e.g. Solomatov and Stevenson, 1993); however, there is some evidence for a protracted freezing sequence (e.g. Abe, 1997; Debaille et al., 2009). Despite difficulties in modelling magma ocean processes generally, and freezing explicitly, we take the starting point of our evolutionary models immediately after the magma ocean crystallisation.

Few previous mantle convection studies have explored setting different initial conditions with similar boundary conditions, even for steady state convection scenarios. For simplicity, we start our model close to the mantle solidus. A justification for this is that the convection pattern may not have yet developed on such a young planet, let alone have reached any stable state, and so a thermal profile coincident with the solidus may be most akin to reality. Perturbations on the initial temperature and lithospheric thickness are also included to facilitate the rapid onset of active convection. There are, however, large uncertainties in initial tem-

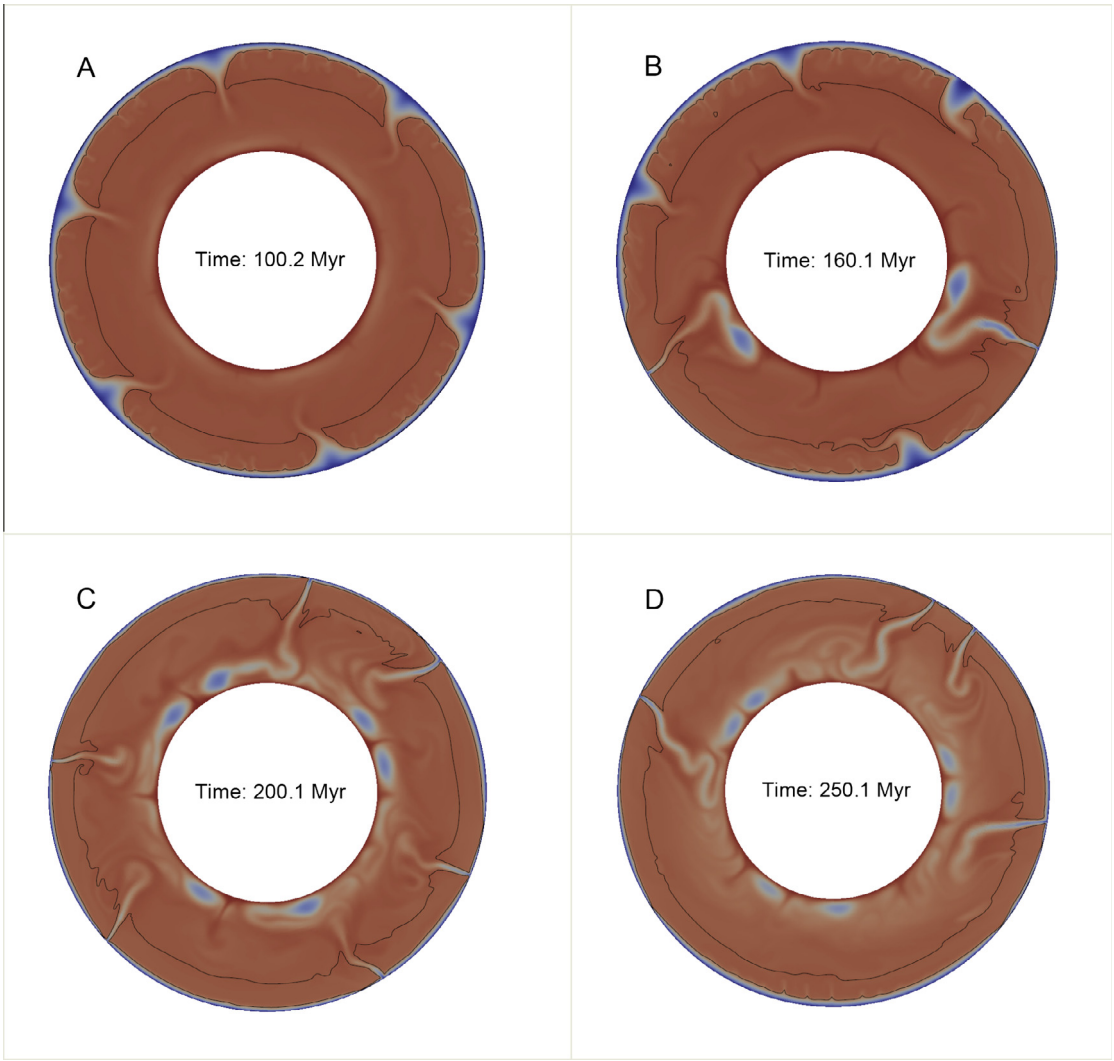

Fig. 9. Main evolution features of model Fric2. Melt fraction is shown in black contour for 50% melt.

peratures and the convection pattern at this stage which requires further investigation, and will be explored through a parameter sweep.

Most evidence suggests that Mars has been in a stagnant-lid regime since around 4.0 Ga. This stagnant-lid stage has been studied extensively in the past, and here we are focussing on the viability of tectonic events in early martian history. Consequently, in this study we only run our models to 800 Myr (3.7 Ga), and consider any later mobile-lid activity after 800 Myr less favourable.

3. Results

3.1. Mobile-lid vs. stagnant-lid

There are three key components which control the likelihood of plate tectonics on terrestrial planets. The first is the thermal contrast of the system, which provides the buoyancy force to drive convection. Second is the yield stress, which controls the lithosphere strength, and third is the viscosity contrast across the system, which controls the partitioning of convective stresses into the lithosphere.

On account of its smaller size, Mars has evolved a smaller thermal contrast over its mantle than Earth. Hotter initial conditions (than at present) would also have resulted in a larger viscosity contrast. Both factors work against active tectonics on Mars.

However, if lithospheric yielding is in place, with the model parameters we have chosen above, the model exhibits mobile-lid behaviour from its onset, immediately post-magma-ocean (Fig. 2). The mantle viscosity increases due to the cooling of the mantle, subduction becomes less active and eventually shuts off at some point, and convection falls into a stagnant-lid regime. This produces high core–mantle boundary heat fluxes in early times, concurrent with active subduction, and a decrease later on.

With our core parameters, the critical heat flow to drive a geodynamo is calculated to be 22 mW/m^2. However, the uncertainties in this value are at least of a factor of 2 (Nimmo and Stevenson, 2000). Another way of determining the possibility of a dynamo is to use the excess entropy (Eq. (13)), especially when there is a growing inner core. The minimum excess entropy that leads to a certain dynamo is not well determined; however, the suggestion of Nimmo et al. (2004) that for an Earth core that any positive value may possibly power a dynamo leads us to consider a dynamo favourable whenever the excess entropy is positive. As shown in Fig. 3B, CMB heat flow indicate that an early mobile-lid model also favours an early dynamo prior to 4 Ga, as suggested by Weiss et al. (2002). The entropy production formulation also suggests a similar result.

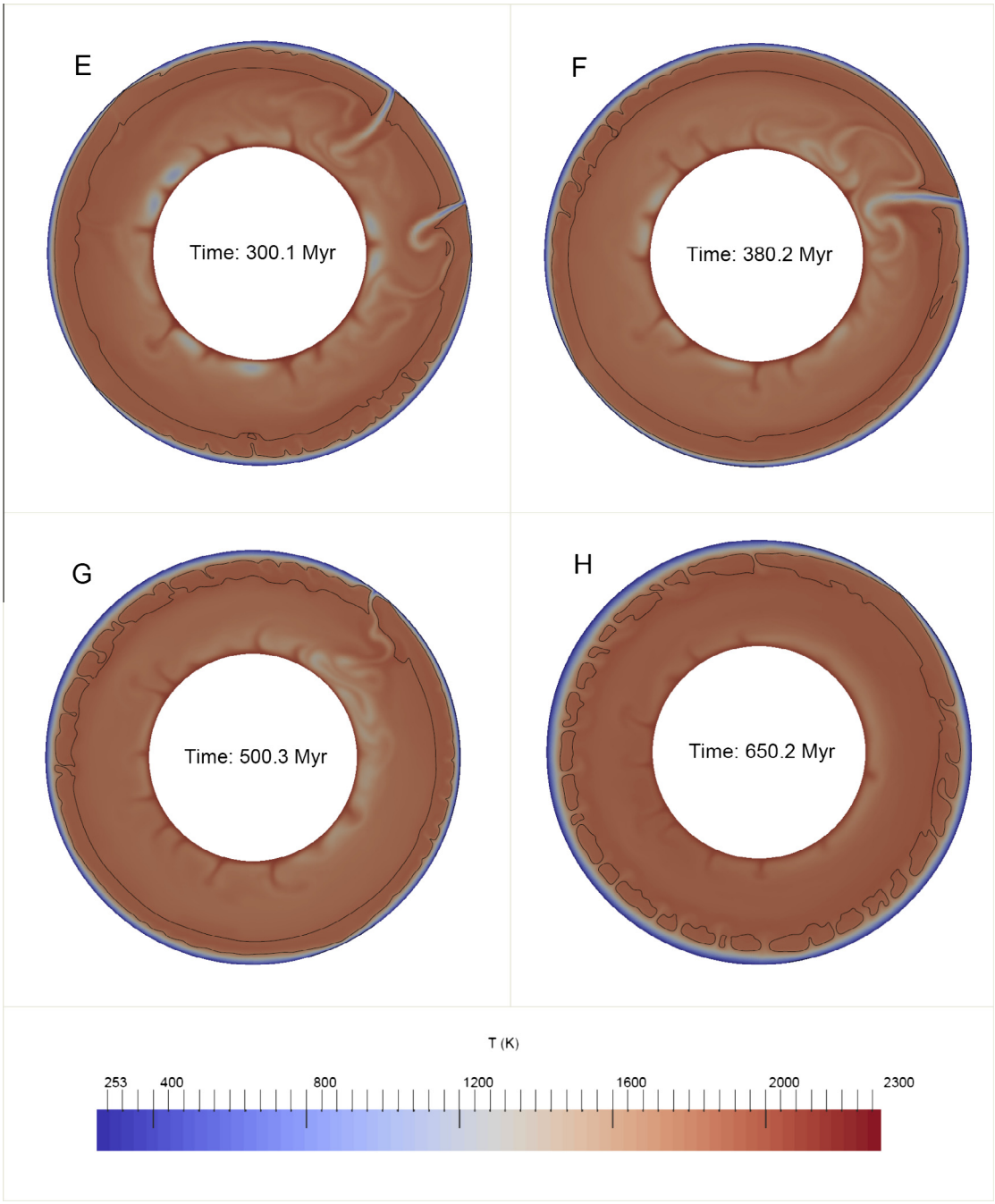

Fig. 9 (*continued*)

With high surface yield stress, mantle convection falls into a stagnant-lid regime from the start. For a stagnant-lid model without a hotter core (**Stag1**), the core cooling rate is quite slow, the core–mantle boundary heat flux is always relatively small and the system barely has enough CMB heat flux required to power a geodynamo (Fig. 3). As such, the magnetic field is likely to be both weak, and in existence only for a very short period of time. The surface heat flux is also much lower compared to the mobile-lid model (as shown in Fig. 3B). The model **Stag2** is similar to **Stag1**, but has a 200 K hotter core. Though the surface heat flux is roughly equivalent to **Stag1**, the heat flux through CMB is much larger. While the CMB heat flux is less than the mobile-lid model, it is likely to be able to support a short dynamo in the first ~100 Myr. The surface heat flux of the mobile-lid model is more than 4 times more efficient than the stagnant-lid counterpart, which results in a much faster cooling of the mantle.

We have also calculated melt production, assuming the melt fraction is a linear function of the difference between the super-solidus temperature, and the mantle solidus, divided by the difference between mantle solidus and liquidus, given by Longhi et al. (1992). The melt production is calculated here without considering melt depletion of the mantle and latent heat effects, and is certainly an over-estimation of the production rate. It is also difficult to generalise about global crustal production from 2D models. As a result, we consider the melt generation to be a more qualitative reflection of its evolution over time, instead of an actual value.

While the mobile-lid models show a massive melt production rate in the early stages of their evolution (around first 300 Myr),

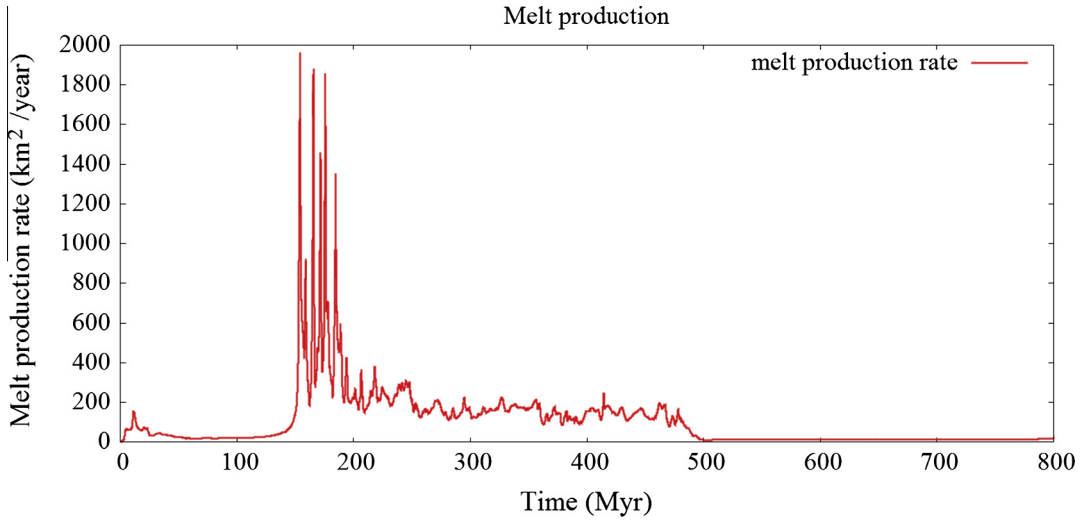

Fig. 10. Melt production rate of model **Fric2**.

they decrease to much lower values in their later stages. The stagnant-lid models, on the countary, show lower melt production rates in their early stages, and higher production rates in later on. Due to the additional heat from the core, the **Stag2** model has even higher late stage melt production rates. Additionally, the overlap of major melt production and dynamo activity is distinctively different between early mobile-lid and stagnant-lid scenarios. While early mobile-lid tectonics produces major melting while the dynamo is still active, the stagnant-lid models produce most of their melt after the dynamo activity has stopped.

When the martian core has very low S content, the core solidus and adiabatic may converge (i.e. allowing the existence of an inner core). As a result we also tested a model with inner core growth, for a stagnant-lid condition. However, the core solidus we are using increases more slowly than the core adiabat. This is likely to result a 'snowing core', i.e. the solidification starts from CMB instead of the centre of the core (e.g. Stewart et al., 2007). The dynamics of this effect, however, cannot be modelled with current parameterization, so we approximated the effect by using an artificial core solidus that increased slightly faster than the core adiabatic. Interestingly, our models show that although inner core growth can last an extremely long time (>800 Myr), the core dynamo can only be active for about 500 Myr. This is different from Williams and Nimmo (2004)'s models, which suggested a longer lasting dynamo time, with a stagnant-lid, superheated core, and with inner core growth. However, we note that both studies use an artificial core solidus, which is not likely to fit the experimental data well. Nonetheless, our results suggest a model with a high inner core growth-rate in the early stages of its evolution, would almost certainly end up with an almost solidified core, which is not considered to be a favourable outcome.

3.2. Different initial conditions

While large uncertainties in initial conditions exist, here we have explored models with different initial temperature profiles. The reference model **Ref** uses temperature profile 30 K less than mantle solidus given by Longhi et al. (1992). The purpose of choosing this instead of the exact mantle solidus is to avoid huge initial mantle remelting at the start of the model. The model **Init1**, however, uses a mantle temperature 200 K cooler than the reference model, while **Init2** uses a mantle temperature 200 K hotter (see Fig. 4). Although a high melt fraction exists in **Init2** model, we have not considered melt extraction or viscosity reduction due to melting explicitly.

For a cooler initial mantle, the viscosity increases and thermal contrast decreases, and these combined effects reduce the likelihood of mobile-lid convection. It takes a much longer time for lithospheric thickening to generate sufficient negative buoyancy to make lid-mobility favourable – and one overturn is observed to occur at times >400 Myr. This system, however, favours an episodic regime of convection, where lid recycling occurs as discrete, punctuated events (e.g. O'Neill et al., 2007b), instead of continuous plate-tectonics (see Fig. 5A).

For a hotter initial mantle, the significant decrease of viscosity results in larger viscosity contrasts between the lithosphere and the underlying mantle. This decreases the lithospheric stress, resulting in plate-tectonic activity decreasing faster compared to the reference model (see Fig. 5B).

Interestingly, model **Init1** exhibits two peaks in CMB heat flux, and thus magnetic intensity (Fig. 6B). The first is due to rapid cooling of the mantle and core. Here, the surface does break and a single ridge is formed at around 100 Myr. However, no subduction occurs, and spreading is taken up by broad, gradual lithospheric thickening that continues until the onset of an overturn event at around 600 Myr. This results in a pulse of heat flux at the core–mantle boundary due to the arrival of cold subducted slabs at that interface, which could potentially result in an increase in magnetic field intensity, and thus a late-onset geodynamo. The CMB heat flux is large, compared to the pure stagnant-lid model **Stag1**. Such high heat fluxes cannot be sustained, however, and the model subsequently evolves into a stagnant-lid regime, without a magnetic field.

A mantle overturn, during the magma-ocean freezing process, and before solid-state mantle convection starts, is also a possible scenario for the initial condition. So here we tested an approximate 'overturned solidus' temperature profile in model **Init3**. As the cold overturned material suppresses generation of stronger plumes, the model falls into the stagnant-lid regime (see Fig. 5C). One limitation of this initial condition is that while it replicates the mantle temperature profile post-overturn, it does not replicate the strong flow-field associated with this event, which restricts its capacity for subsequent tectonics. It also boosts the initial CMB heat flux, which is likely to be able to power a very brief dynamo. After that it behaves similarly to other stagnant-lid models discussed before. The dynamo lifetime is relatively short in this model, which provides another possibly testable evolutionary scenario.

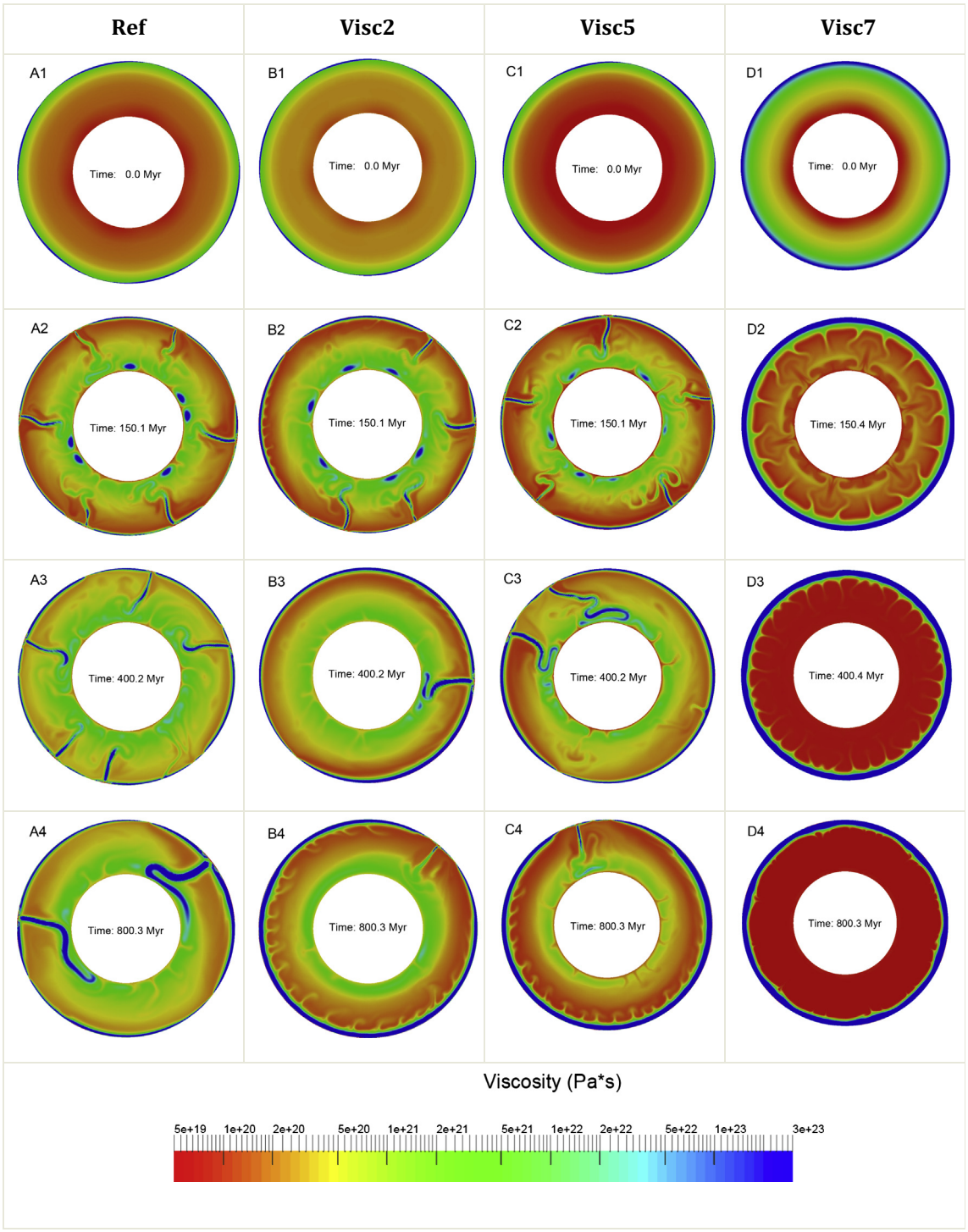

Fig. 11. Model evolution for different rheological parameters. The reference model **Ref** has an activation energy of 157 kJ/mol, and an activation volume of 1.5 cm^3/mol. Model **Visc2** has an activation volume of 2.0 cm^3/mol, and model **Visc5** and **Visc7** have activation energies of 200 kJ/mol and 300 kJ/mol respectively (other values as per **Ref**).

3.3. Variation of yield stress

Yield stress has a key role in controlling the surface mobility. The yield stress on early Mars depends on surface water and other factors which are poorly constrained. In the models shown before (Fig. 2), a very low friction coefficient 0.08 is used as reference value to make sure a mobile-lid regime is achieved. Here we explored a range of higher friction coefficients, from 0.10 (**Fric1**), to 0.12 (**Fric2**), and 0.15 (**Fric3**), as shown in Fig. 7.

When the friction coefficient is increased from 0.08 (**Ref**) to 0.10 (**Fric1**), little variation is observed in the evolutionary path. The first overturn happens very early, and is followed by a subduction system similar to conventional Earth-like tectonics. Plate activity decreases with time, resulting in fewer subducting slabs. However subduction also ceases earlier with a higher friction coefficient. Although the convection pattern looks similar at 150 Myr in models **Ref** and **Fric1**, there is only one slab left in the **Fric1** model at 400 Myr (Fig. 7), while the **Ref** model has numerous active

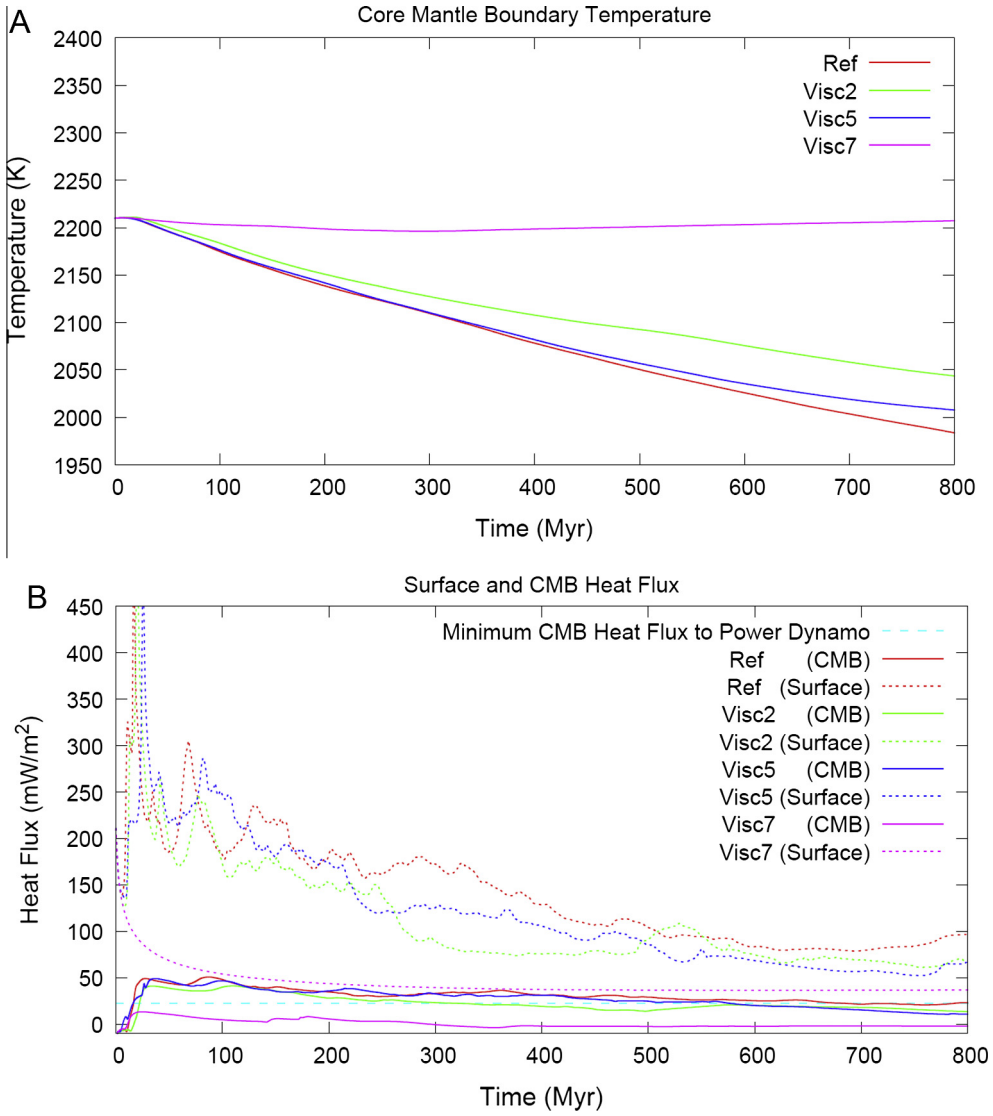

Fig. 12. Evolution of core–mantle temperature (A), and heat flux (B) for models with different rheological parameters **Ref**/**Visc2**/**Visc5**/**Visc7** (see text for description).

subduction zones (Fig. 2). The CMB heat flux is above the minimum value for possible dynamo activity for the first 500 Myr (Fig. 8).

For the model **Fric3** we use coefficient of friction 0.15 which results in a late overturn after 600 Myr (Fig. 8). The CMB heat flux of this model is not enough to generate a dynamo before the overturn. Although the overturn event boosts the heat flux and makes a dynamo possible, the timing of the dynamo-generated field in this example is later than that inferred for Mars.

The most interesting model of this test is the **Fric2** which uses friction coefficient 0.12. As a result of increasing the yield stress, the model's evolution occurs in four different stages. Stage **I** is from 0 to 160 Myr. During this stage, a surface boundary layer develops (Fig. 9A), and while a few ridges are observed, no subduction zones form. Core cooling is slow in this stage, and the CMB temperature drop is close to both model **Fric3** (Fig. 8A) and the stagnant-lid model **Stag1** (Fig. 3A). The heat flux through the CMB is slightly higher in this model when compared to **Fric3** (Fig. 8B), and is likely to have been large enough to power a brief dynamo in this stage. Stage **II** is defined by the onset of the first regional overturn between 160 Myr and 200 Myr (Fig. 9B). At the cessation of this stage the overturn event has progressed to a global scale, and a subduction system is fully developed (Fig. 9C). Although the Stage **I** dynamo should have been extinct at the onset of this overturn, the rapidity of slab subduction provides an immediate boost to the CMB heat flux (Fig. 8B), and results in high entropy production – restarting the dynamo. After 200 Myr, the model enters stage **III** which is characterised by a period of more continuous plate tectonics. Similar to the model **Ref**, the mantle viscosity increases slowly with time due to the cooling of the mantle. The activity of subduction decreases through time; there are 6 slabs at 200 Myr (Fig. 9C), this is reduced to 4 slabs at 250 Myr (Fig. 9D), 2 slabs at 300 Myr (Fig. 9E), and a single slab left at 380 Myr (Fig. 9F), until subduction ceases at around 500 Myr (Fig. 9G). The CMB heat flux (Fig. 8B) slowly wane during this stage, due to the decreasing plate tectonic activity of the mantle. However it is still possible to maintain an active dynamo throughout most of this stage. After the last slab dies at around 500 Myr (Fig. 9G), the model reaches stage **IV** which is a stagnant-lid-like convection mode. Although subduction has ceased, there is still an active ridge until the end of our simulation at 800 Myr (Fig. 9H). The heat flux through the CMB is no longer high enough to drive an active dynamo in this stage (Fig. 8B). The second peak in CMB heat flux is tightly coupled to plate tectonic activity, which suggests that the early martian dynamo may be highly correlated to the mobility of the surface.

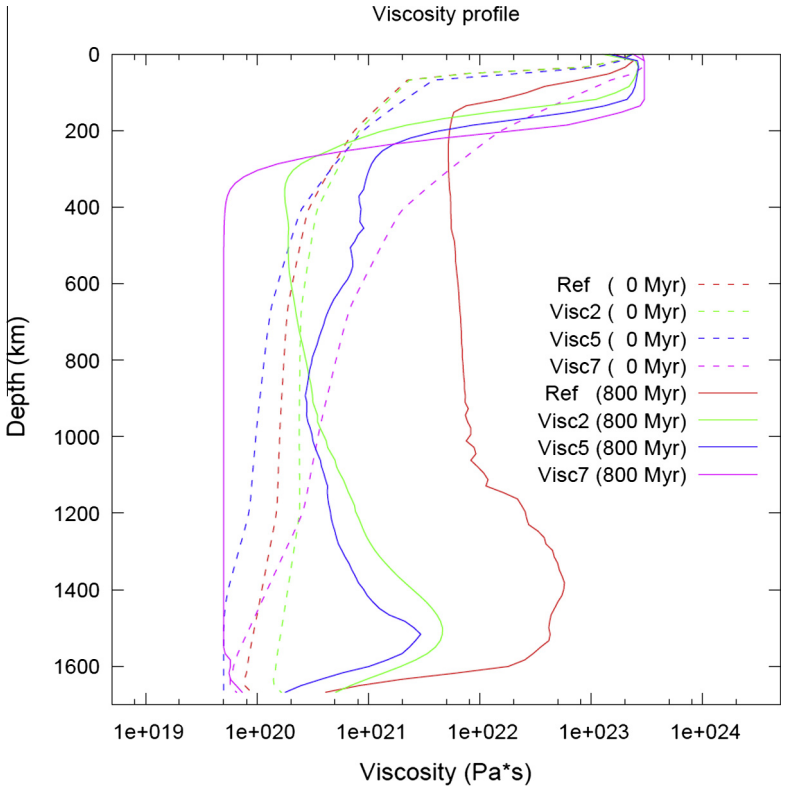

Fig. 13. Evolution of viscosity profile between the initial (0 Myr) and end simulation (800 Myr) of models with different rheological parameters **Ref**/**Visc2**/**Visc5**/**Visc7** (see text for description).

There is a strong link between melt production and surface mobility as well. In this model, we observed a small peak in melt production rate at around 10 Myr when the initial plumes rise. When the first overturn event occurs, the melt production receives a huge boost almost immediately, and after surface mobility decreases and finally falls into a stagnant-lid regime, the melt production decreases accordingly (Fig. 10).

3.4. Variation of activation volume and activation energy

Given that large uncertainties exist in mantle rheological parameters, we explore a range of activation volume and activation energy values, and study their impact on model evolution.

Activation volume under higher pressure is very poorly constrained; in the reference model we use relatively low effective activation volumes of $\sim$1.5 cm^2/mol. However higher values are suggested by experiments in low pressure and much higher strain rate conditions, and a value of 3–4 cm^2/mol is used by many previous models using similar rheology (e.g. Roberts and Arkani-Hamed, 2012; Tosi et al., 2013; Sekhar and King, 2014). Here we test an activation volume of 2.0 cm^2/mol (model **Visc2**) in comparison with the reference value 1.5 cm^2/mol. Due to the increase of activation volume, there is a noticeable increase in lower mantle viscosity (model **Visc2**) compared to reference model **Ref** (Fig. 11). Although it doesn't delay the overturn and the initiation of subduction too much, the increased lower mantle viscosity suppresses the likelihood of mobile-lid convection, and results in a noticeably earlier cessation of subduction. While the reference model still has two slabs left at 800 Myr, the last slab of **Visc2** is almost moribund, and a much thicker lithosphere has developed which indicate this model is closer to entering into a stagnant-lid regime.

The effective activation energy we chose for our reference model was calculated based on the dislocation creep of wet olivine from Karato and Wu (1993), and similar values are also used in many other models (e.g. Roberts and Zhong, 2006; Sekhar and King, 2014). However due to the uncertainties in activation energy, higher values are also used in other studies (e.g. Tosi et al., 2013). Here we explore models with activation energies of 200 kJ/mol (**Visc5**), and 300 kJ/mol (**Visc7**). While increasing the activation energy, the pre-exponent factor A in Eq. (5) is also changed accordingly to get the similar initial mantle average viscosity. Increasing the activation energy to 200 kJ/mol slightly increases the viscosity contrast between lithosphere and underlying mantle which reduces the likelihood of mobile-lid convection. The evolutionary path is quite similar to model **Visc2**, which has an increased activation volume. Although increasing activation volume and activation energy have different influences on the viscosity structure (the former increases the lower mantle viscosity and latter increases the viscosity contrast between lithosphere and mantle), both of those changes reduce the likelihood of mobile-lid behaviour. The parameters of our reference model are rather close to the transition between mobile-lid and stagnant-lid. Decreasing the likelihood of mobile-lid behaviour results plate-tectonics activity ending earlier (Fig. 11). The CMB temperature reductions of **Visc5** and **Visc2** are not significantly different compared to **Ref**; **Visc5** and **Visc2** CMB temperatures exhibit only a marginally smaller drop compared to **Ref**, with **Visc2** being the lesser of the two (Fig. 12A). The heat flux throughout the core also show a small reduction in both **Visc2** and **Visc5** (Fig. 12B).

The evolution of average viscosity profile for different models is shown in Fig. 13.

Although slight changes in rheological parameters do not alter the evolutionary path significantly (as shown in model **Visc2** and **Visc5**), increasing activation volume to 300 kJ/mol (shown in model **Visc7**) will significantly lower the mantle viscosity and create huge viscosity contrasts between lithosphere and mantle that completely push the model into a stagnant-lid regime over the entirety of its run time. No significant core cooling is observed in

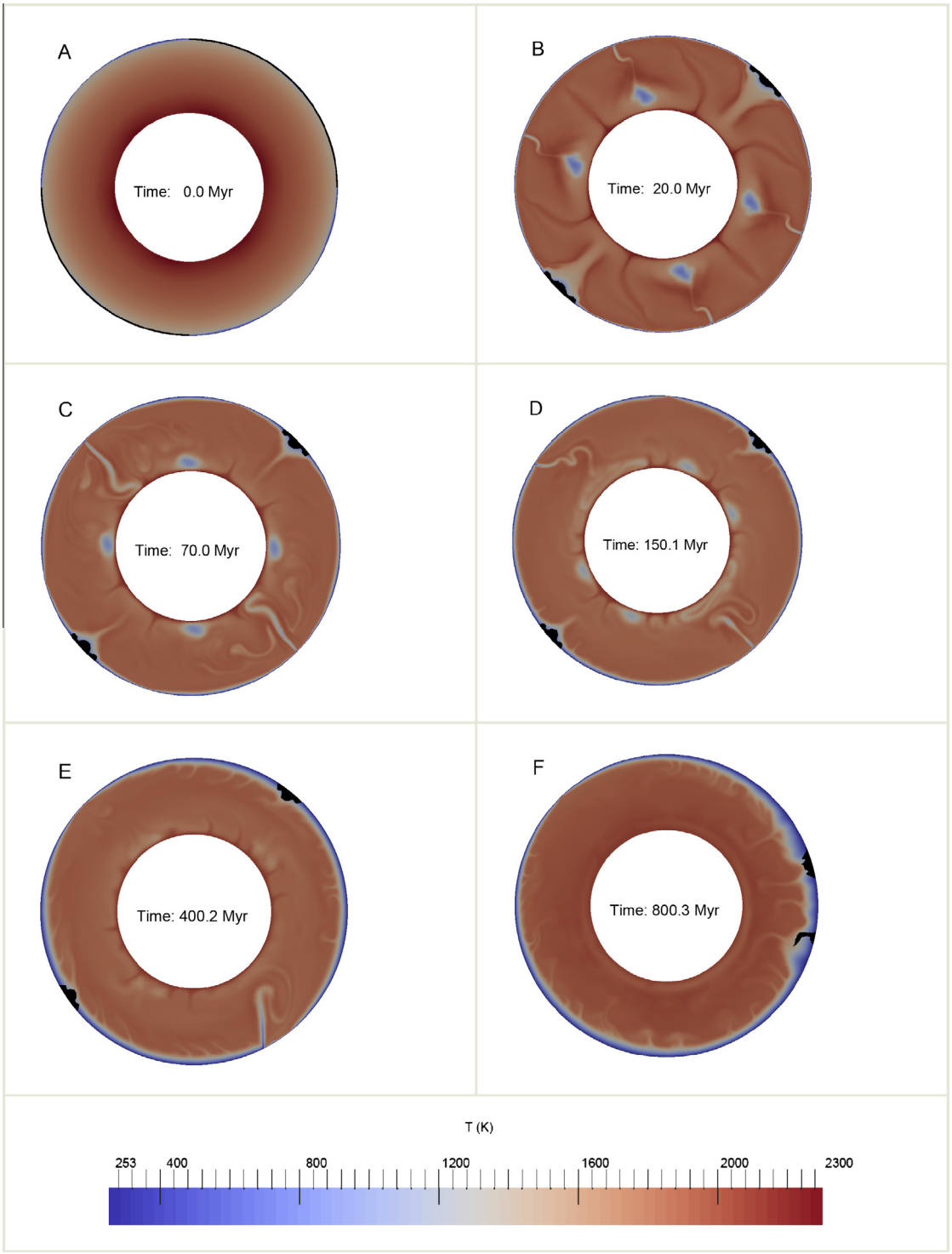

Fig. 14. Model evolution including an initial buoyant crustal layer which is 200 kg/m^3 more buoyant than the mantle; other parameters are the same as the reference model **Ref**. The black colour marks the area that has 50% or more crustal materials.

this model and the CMB heat flux is not large enough to reach active dynamo conditions (Fig. 12).

3.5. Impact of existence of the crust

In the previous models, there were no compositional differences in the convection system. However, the primitive martian crust may have already formed in the first 100 Myr of martian history (e.g. Humayun et al., 2013). The existence of a compositionally different crust may have a strong impact on the mantle dynamic behaviour. To test this, we built a preliminary test model with two thin (30 km) initial crustal blocks that cover half of the planet surface, to simulate the behaviour of continents. The crust is 200 kg/m^3 more buoyant than the mantle, and for simplicity, the

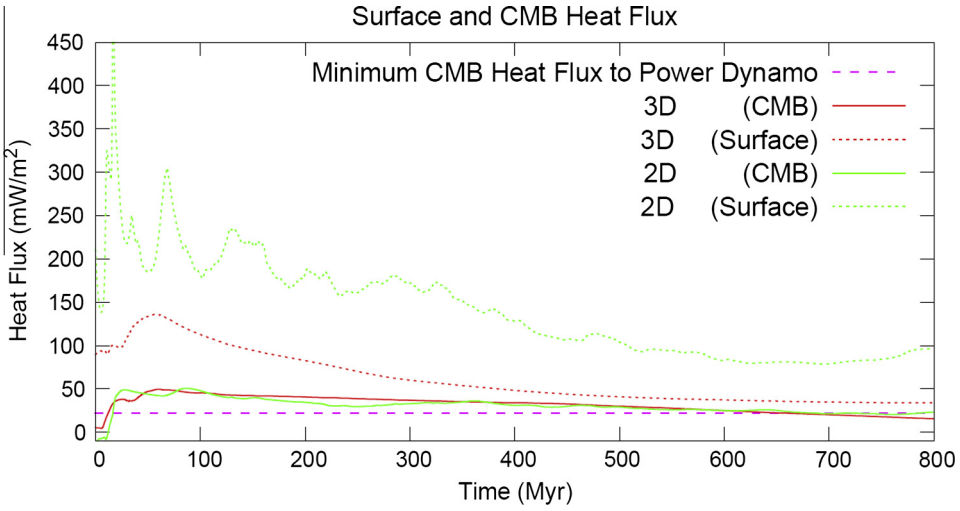

Fig. 15. Heat flux comparison between 2D and 3D mobile-lid models.

rheological differences between the mantle and the crust are not considered in this model. After introducing the buoyant crust, the subduction pattern is predominantly controlled by the existence of continents. While starting with six initial plumes in the same manner as the model **Ref**, the four slabs that are initiated by the overturn are quickly combined into two slabs due to the geometric controls of the continents. Buoyant continents also reduce the likelihood of mobile-lid behaviour. One of the two slabs dies out at around 400 Myr and the other around 550 Myr, and the models enter into a stagnant-lid regime (Fig. 14). In comparison, the model **Ref**, with same parameters, except for the buoyant crust, still has many slabs active at 400 Myr and 2 slabs active at 800 Myr (Fig. 2). From our test model, while introducing buoyant crust will not prevent the model from entering into a mobile-lid, it will help to shut off mobile-lid convection and force the system to enter into a stagnant-lid more quickly, as suggested by Lenardic et al. (2004). However, we consider this model quite preliminary, as the density difference between the crust and mantle is likely too small, and no other differences in material parameters (i.e. thermal conductivity, internal heating rate, and strength) were considered.

3.6. Differences between 2D and 3D

All our previously models shown here are in 2D. Although the code ASPECT allows easy transitions for 2D model into 3D with the same settings, high resolution, longer term 3D models are quite computationally expensive, especially when using more complex rheologies. Here we have managed to run a 3D mobile-lid model with reduced resolution using similar parameters as the previous 2D model **Ref**. The 3D model exhibits a similar evolutionary path to its 2D counterpart. The continuously high CMB heat flux (Fig. 15) indicate a long-lived active dynamo. This dynamo is likely to shut off at around 650 Myr in a manner similar to the 2D model **Ref**. The evolutionary path is shown more clearly in Fig. 16. In the early stages (~100 Myr), plates are forming, and subduction zones and ridges are active due to low viscosity zones created by plastic yielding. As the model further develops, a significant reduction in surface yielding is observed. Although some weak boundaries still exist, subducting slabs stop penetrating deep into the mantle, and the multiple plate system in existence at 100–200 Myr becomes frozen into a single plate planet at 800 Myr. Most of the behaviour is similar between 2D and 3D models, however there are still some differences. Although the models exhibit similar CMB heat fluxes, the surface heat flux of the 3D model is only about half of the 2D counterpart. The reason is geometrical: the ratio between the CMB area: surface area changes from ~2 (in 2D) to ~4 (in 3D). The volume/surface area ratio for internal heating also changes, but this change is much smaller than the surface/CMB area ratio change. As a result, the top surface in 3D would be expected to lose heat twice efficiently than in 2D, and the surface heat flux reflects this difference. Differences in model dynamics are also observed. For example while the 2D model has clearly evolved into a two slab system at 800 Myr, in the 3D model, the slab systems have already died out, as a result of greater frictional (toroidal) dissipation in 3D. However a ridge is still operating, and the model is also more likely to evolve into a degree one convection system, which may create a martian hemisphere dichotomy as suggested by Roberts and Zhong (2006). In short, differences between 2D and 3D models include changes in heat flux balance, plate dynamics, and convection intensity. Differences in the timing of the transition in convection regime would be expected when changing from 2D into 3D (due to, for example, transform fault motion), and will require further investigation.

4. Discussion and conclusions

The series of models outlined above illustrate the physical plausibility, and restrictions, of tectonics on an evolving Mars-type planet. A range of uncertainties in model set up exist, and variation in parameters such as rheology, initial conditions, and compositional differences of the crust have been explored. Increasing the friction coefficient, activation energy, activation volume, and introducing a buoyant crustal layer all slightly reduce the likelihood of mobile-lid tectonics, and change the timing of the stagnant-lid transition. Varying those parameters within uncertainty ranges, however, does not significantly alter the evolutionary story.

We were able to construct models that possessed early mobile-lid tectonics on Mars, in the first half billion years or more, and which later evolved into a stagnant-lid regime. Core cooling is tightly associated with surface mobility, and early mobile-lid models are likely to produce a dynamo history in accordance with the paleomagnetic field studies of the martian crust (Acuna et al., 1999). While Lenardic et al. (2004) suggested a mobile-lid shut-off due to growth of the Southern Highlands, we found the plate-tectonics may have simply shut off due to thermal cooling. Our models support the findings of Williams and Nimmo (2004) parameterized study, and are able to reproduce an early dynamo in pure stagnant-lid models with a superheated core – albeit with

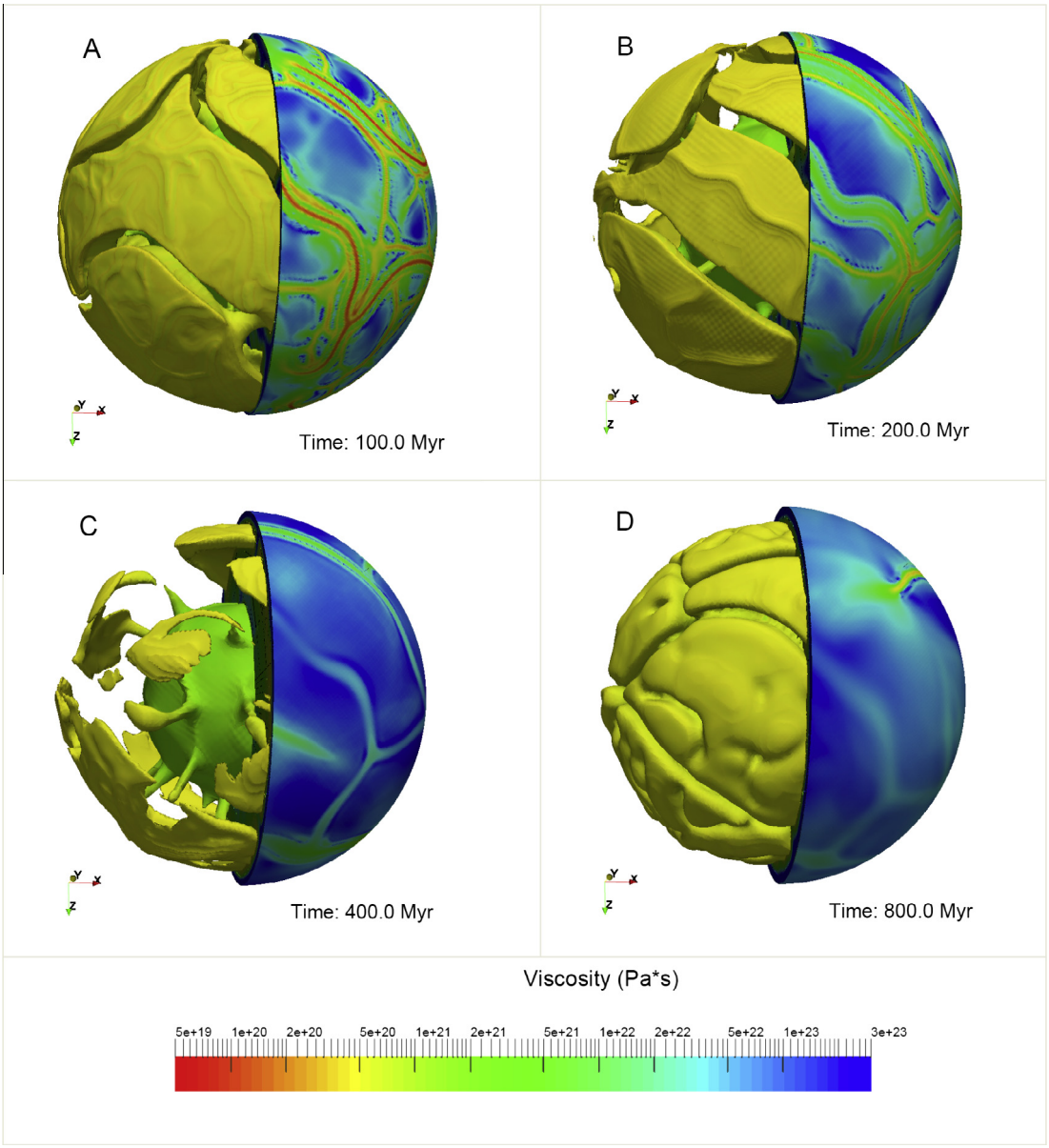

Fig. 16. Evolution of a 3D mobile-lid model. The colour here shows the viscosity. The half sphere on the left of each figure shows the surface viscosity, and the low viscosity zones shows where surface yielding is taking place. The surface on the left of each figure is a temperature isosurface, which shows the evolution of internal structure. (For interpretation of the references to colour in this figure legend, the reader is referred to the web version of this article.)

extremely high late-stage melt production. An early dynamo is also possible for stagnant lid models with an initial 'overturned solidus' condition, or a freezing inner-core. However, our reference stagnant-lid models – without a superheated core – were not able to generate dynamo activity. Whilst variants of both early mobile-lid, and stagnant-lid, are able to produce an early dynamo, the melt production histories are totally different. Early mobile-lid scenarios result in massive melt production in the first few hundred Myrs, which wanes with time. The stagnant-lid models, in contrast, produce massive melting only after a few hundred million years. A similar argument was made Breuer and Spohn (2003), who in fact favoured stagnant-lid for the later peak melt production. In our models, however, we found that although an early mobile-lid has peak melt production in its early stages, it still has lower, but significant, melt production in its later evolution, whilst the melt production for stagnant-lid models in their later stages (~Amazonian) is larger than their initial evolution, which is at odds with existing constraints on martian crustal production (e.g. Greeley and Schneid, 1991). Other models that produce less melt in a stagnant-lid regime start their model from a cooler condition, instead of our initial condition close to the mantle solidus (Breuer and Spohn, 2003; Ruedas et al., 2013; Sekhar and King, 2014). Furthermore, stagnant-lid cooling may be more efficient if a 'heat pipe' mechanism is included (Moore and Webb, 2013), and repartitioning of heat producing elements into the crust during melting process incorporated (O'Neill et al., 2005). Future work should include a more detailed treatment of the melting process (e.g. Ruedas et al., 2013) to further investigate this problem. Additionally, in our stagnant-lid models, the peak in crust production occurs when there is no magnetic field, which is not likely to be true as the majority of the Southern Highland crust is believed to be ancient, and large portion of it is suggested to be formed contemporaneously with an active dynamo (Acuna et al., 1999; Connerney et al., 1999).

In our stagnant-lid models, we only produced smaller-scale convection features, instead of a degree-one plume. A stratified mantle viscosity (Zhong and Zuber, 2001; Roberts and Zhong, 2006), or spinel-perovskite structure phase change close above the CMB (Harder and Christensen, 1996; Breuer et al., 1998) are possibilities in generating degree-one features, and were not incorporated here. However the stratified mantle viscosity requires a very large viscosity contrast between lower and upper mantle, which may not be justified. And whether the phase transition is strong enough to suppress smaller plumes is also under debate (e.g. Ruedas et al., 2013). Keller and Tackley (2009) were able to generate hemispheric crustal thickening above one-ridge spreading systems. In many of our early mobile-lid/episodic models, we also end up with larger-scale degree-1 lithospheric features in the later stages, as a result of global asymmetries in the subduction and ridge systems.

Another key feature of Mars' dynamic evolution is the formation the Tharsis Rise, which lies near the dichotomy boundary, and which most of the present models failed to produce. Van Thienen et al. (2006) try to explain this by top down convection with an active lid on the northern hemisphere. Zhong (2009) and Šrámek and Zhong (2010) trying to explain this by super plume initiated underneath Southern Highlands, and later migrated to dichotomy boundary by lithosphere rotation. In our early mobile-lid/episodic models, we do see rapid motions of surface blocks, and small plumes swept up by cold top-down flows while the surface is active. The plumes become more stationary once surface mobility reduced. The later stages of our episodic model **Fric2** shows a single ridge with a one-hemisphere diffusive deformation zone, and a thickened and stronger lithosphere at another. However without predefining the hemispherical lithosphere cap, the ridge sits almost symmetrically in the middle. Including of compositionally distinct crust, which can result in deeper continental roots capable of modulating the convection pattern, may break this symmetry. In one of our test models with two predefined crustal blocks, we observed that the interference of thick crustal blocks may help to break the symmetry of the system, and relocate the volcanic system closer to the dichotomy boundary.

Although most research agrees that Mars had an early magnetic field, the timing of the window for an active dynamo is still poorly constrained. Acuna et al. (1999) suggests a cessation time at around 4.0 Ga, while Schubert et al. (2000) argues for a late start of the dynamo. Weiss et al. (2002) posits that the dynamo was active at around 3.9–4.1 Ga by studying martian meteorite ALH84001, and Lillis et al. (2013) suggests that the dynamo ceased before 4.0–4.1 Ga. A recent study by Milbury et al. (2012) argues for a cessation time around 3.6 Ga. In our models, the mobile-lid tectonics favours an early start and longer lasting dynamo, while the episodic models can produce a delayed start with multiple dynamo-active windows also possible. We found that the core dynamo and melt production rate are highly associated with surface mobility. As recent work by Halevy and Head (2014) suggests punctuated volcanism continued till approximately 3.7 Ga, and this may favour a protracted tectonic evolution of early Mars as well.

In our models, the operating time for surface mobility also varies due to model parameter uncertainties such as yield strength, initial conditions, and rheology. If early mobile-lid/episodic convection occurred on Mars, the surface was likely to be mobile only in the very earliest stages of its evolution, may not have lasted as long as some of our models. Our results indicate increasing yield strength will both hasten the shutoff, and delay the start of the overturn as well. We did not include a stratified density structure, as have been suggested due the fractional magma-ocean crystallisation. The overturn of an unstably stratified mantle may in effect kick-start rapid early tectonics, and may facilitate an early start even with high yield strengths. So although in our current models the active mobile surface can start in a few tens to hundreds of Myrs or more, and last for a few hundred Myrs, an earlier start, or earlier shutoff, is also quite possible.

There are a few limitations of our models that need to be addressed in future studies. Firstly, detailed treatment of melting, and crustal generation processes, need to carried out to address heat lost due to melt transport, and the partitioning of heat production elements during crustal growth, which is absent in our model. Secondly, more practical rheologies need to explored, currently we only use a Newtonian viscosity with a relatively narrow viscosity cut-off, and plastic yielding. Thirdly, the effect of giant impacts in early martian history that may have a strong influence on the evolution of the planet, and need to be addressed. Lastly, most of our models are tested in 2D, the differences between 2D and 3D need to be further explored.

In conclusion, although large uncertainties exist for both early Mars and the rheological parameters used, we have identified a range of circumstances under which early Mars may have exhibited early mobile-lid tectonics, or episodic overturn events. Whilst the question of whether or not Mars itself possessed active tectonics still remains unresolved, the behaviours we observe in tectonically active models are able to satisfy martian dynamo, and crustal production constraints. We also found a strong link between surface mobility and core dynamo activity in our models, which may be an important generalisation for understanding planetary evolution. Due to the reasons discussed above, we favour a scenario that is close to our **Fric2** model. An overturn may have occurred early (a few tens of Myrs to ~100 Myr after magma-ocean crystallisation), to be subsequently followed by a short period of plate-tectonics, which shutoff within a few hundred Myrs. During the window that the surface is actively mobile, the majority of crustal production occurs, contemporaneous with dynamo activity. During this fast initial cooling of the mantle, low degree convection features – a consequence of slab dynamics – become dominant. Crust is preferentially thickened in one hemisphere, forming a terrane reminiscent of the Southern Highlands. As the model evolves most smaller plumes die out, leaving only one major plume/ridge. This final upwelling may be relocated to its final location by either the dynamics of downwellings, or lithospheric rotation, to finally form the Tharsis volcanic province. After the surface ceases to be mobile, the position of this plume is likely to remain relatively stationary, and volcanically active for quite a long time.

In this study, we confirm that an early convection regime shifts from mobile-lid/episodic to later stagnant-lid is plausible for a Mars-like planet. Such an evolutionary path results in both an evolving dynamo history, and a melt production rates, that are consistent with martian magnetic history constraints, and estimates of crustal production.

Acknowledgments

This is contribution 675 from the ARC Centre of Excellence in Core to Crust Fluid Systems (www.CCFS.mq.edu.au) and 1039 from the GEMOC Key Centre (http://www.GEMOC.mq.edu.au). This research was undertaken with the assistance of resources provided at the NCI National Facility systems at the Australian National University and INTERSECT through the National Computational Merit Allocation Scheme supported by the Australian Government. CO was supported by ARC grants FT100100717 and DP110104145.

References

Abe, Y., 1997. Thermal and chemical evolution of the terrestrial magma ocean. Phys. Earth Planet. Inter. 100, 27–39.

Acuna, M.H. et al., 1999. Global distribution of crustal magnetization discovered by the Mars global surveyor MAG/ER experiment. Science 284, 790–793.
Andrews-Hanna, J.C., Zuber, M.T., Banerdt, W.B., 2008. The Borealis basin and the origin of the martian crustal dichotomy. Nature 453, 1212–1215.
Baker, V.R. et al., 1991. Ancient oceans, ice sheets and the hydrological cycle on Mars. Nature 352, 589–594.
Breuer, D., Spohn, T., 2003. Early plate tectonics versus single-plate tectonics on Mars: Evidence from magnetic field history and crust evolution. J. Geophys. Res. – Planets 108, 5072.
Breuer, D., Spohn, T., 2006. Viscosity of the martian mantle and its initial temperature: Constraints from crust formation history and the evolution of the magnetic field. Planet. Space Sci. 54, 153–169.
Breuer, D. et al., 1998. Three dimensional models of martian mantle convection with phase transitions. Geophys. Res. Lett. 25, 229–232.
Bürgmann, R., Dresen, G., 2008. Rheology of the lower crust and upper mantle: Evidence from rock mechanics, geodesy, and field observations. Annu. Rev. Earth Planet. Sci. 36, 531–567.
Carr, M.H., 1987. Water on Mars. Nature 326, 30–35.
Christensen, U., 1983. Convection in a variable-viscosity fluid: Newtonian versus power-law rheology. Earth Planet. Sci. Lett. 64, 153–162.
Connerney, J.E. et al., 1999. Magnetic lineations in the ancient crust of Mars. Science 284, 794–798.
Debaille, V. et al., 2009. Early martian mantle overturn inferred from isotopic composition of nakhlite meteorites. Nat. Geosci. 2, 548–552.
Di Giuseppe, E. et al., 2008. Slab stiffness control of trench motion: Insights from numerical models. Geochem. Geophys. Geosyst. 9, Q02014.
Elkins-Tanton, L.T., 2005. Possible formation of ancient crust on Mars through magma ocean processes. J. Geophys. Res. 110, E12S01.
Escartin, J., Hirth, G., Evans, B., 2001. Strength of slightly serpentinized peridotites: Implications for the tectonics of oceanic lithosphere. Geology 29, 1023–1026.
Frey, H., Schultz, R.A., 1988. Large impact basins and the mega-impact origin for the crustal dichotomy on Mars. Geophys. Res. Lett. 15, 229–232.
Greeley, R., Schneid, B.D., 1991. Magma generation on Mars: Amounts, rates, and comparisons with Earth, Moon, and Venus. Science 254, 996–998.
Gubbins, D. et al., 2003. Can the Earth's dynamo run on heat alone? Geophys. J. Int. 155, 609–622.
Gubbins, D. et al., 2004. Gross thermodynamics of two-component core convection. Geophys. J. Int. 157, 1407–1414.
Halevy, I., Head III, J.W., 2014. Episodic warming of early Mars by punctuated volcanism. Nat. Geosci. 7, 865–868.
Harder, H., Christensen, U.R., 1996. A one-plume model of martian mantle convection. Nature 380, 507–509.
Head, J.W., 2002. Northern Lowlands of Mars: Evidence for widespread volcanic flooding and tectonic deformation in the Hesperian Period. J. Geophys. Res. 107, 5004.
Humayun, M. et al., 2013. Origin and age of the earliest martian crust from meteorite NWA 7533. Nature 503, 513–516.
Karato, S.-i., 2010. Rheology of the Earth's mantle: A historical review. Gondwana Res. 18, 17–45.
Karato, S.-i., Wu, P., 1993. Rheology of the upper mantle: A synthesis. Science 260, 771–778.
Ke, Y., Solomatov, V.S., 2009. Coupled core–mantle thermal evolution of early Mars. J. Geophys. Res. 114, E07004.
Keller, T., Tackley, P.J., 2009. Towards self-consistent modeling of the martian dichotomy: The influence of one-ridge convection on crustal thickness distribution. Icarus 202, 429–443.
Kiefer, W.S., 2003. Melting in the martian mantle: Shergottite formation and implications for present-day mantle convection on Mars. Meteorit. Planet. Sci. 38, 1815–1832.
Kronbichler, M., Heister, T., Bangerth, W., 2012. High accuracy mantle convection simulation through modern numerical methods. Geophys. J. Int. 191, 12–29.
Labrosse, S., Poirier, J.-P., Mouel, J.-L.L., 2001. The age of the inner core. Earth Planet. Sci. Lett. 190, 111–123.
Lammer, H. et al., 2012. Outgassing history and escape of the martian atmosphere and water inventory. Space Sci. Rev. 174, 113–154.
Lenardic, A., Nimmo, F., Moresi, L., 2004. Growth of the hemispheric dichotomy and the cessation of plate tectonics on Mars. J. Geophys. Res. – Planets 109, E02003.
Lillis, R.J. et al., 2013. Time history of the martian dynamo from crater magnetic field analysis. J. Geophys. Res. – Planets 118, 1488–1511.
Lodders, K., Fegley, B., 1997. An oxygen isotope model for the composition of Mars. Icarus 126, 373–394.
Longhi, J. et al., 1992. The bulk composition, mineralogy and internal structure of Mars. Mars 1, 184–208.
McGovern, P.J., 2002. Localized gravity/topography admittance and correlation spectra on Mars: Implications for regional and global evolution. J. Geophys. Res. 107, 5136.
McGovern, P.J., 2004. Correction to "localized gravity/topography admittance and correlation spectra on Mars: Implications for regional and global evolution". J. Geophys. Res. 109, E07007.
Milbury, C. et al., 2012. The history of Mars' dynamo as revealed by modeling magnetic anomalies near Tyrrhenus Mons and Syrtis Major. J. Geophys. Res. 117, E10007.
Moore, W.B., Webb, A.A.G., 2013. Heat-pipe Earth. Nature 501, 501–505.
Moresi, L.N., Solomatov, V.S., 1995. Numerical investigation of 2D convection with extremely large viscosity variations. Phys. Fluids 7, 2154–2162.
Moresi, L., Solomatov, B., 1998. Mantle convection with a brittle lithosphere: Thoughts on the global tectonic styles of the Earth and Venus. Geophys. J. Int. 133, 669–682.
Nimmo, F., Stevenson, D.J., 2000. Influence of early plate tectonics on the thermal evolution and magnetic field of Mars. J. Geophys. Res. – Planets 105, 11969–11979.
Nimmo, F. et al., 2004. The influence of potassium on core and geodynamo evolution. Geophys. J. Int. 156, 363–376.
Ogawa, M., Yanagisawa, T., 2011. Numerical models of martian mantle evolution induced by magmatism and solid-state convection beneath stagnant lithosphere. J. Geophys. Res. 116, E08008.
O'Neill, C., Debaille, V., 2014. The evolution of Hadean–Eoarchaean geodynamics. Earth Planet. Sci. Lett. 406, 49–58.
O'Neill, C., Moresi, L., Lenardic, A., 2005. Insulation and depletion due to thickened crust: Effects on melt production on Mars and Earth. Geophys. Res. Lett. 32, L14304.
O'Neill, C. et al., 2007a. Melt propagation and volcanism in mantle convection simulations, with applications for martian volcanic and atmospheric evolution. J. Geophys. Res. 112, E07003.
O'Neill, C. et al., 2007b. Episodic precambrian subduction. Earth Planet. Sci. Lett. 262, 552–562.
O'Neill, C. et al., 2009. Influence of supercontinents on deep mantle flow. Gondwana Res. 15, 276–287.
Ringwood, A.E., Irifune, T., 1988. Nature of the 650-km seismic discontinuity – Implications for mantle dynamics and differentiation. Nature 331, 131–136.
Roberts, J.H., Arkani-Hamed, J., 2012. Impact-induced mantle dynamics on Mars. Icarus 218, 278–289.
Roberts, J.H., Zhong, S., 2006. Degree-1 convection in the martian mantle and the origin of the hemispheric dichotomy. J. Geophys. Res. 111, E06013.
Ruedas, T., Tackley, P.J., Solomon, S.C., 2013. Thermal and compositional evolution of the martian mantle: Effects of phase transitions and melting. Phys. Earth Planet. Inter. 216, 32–58.
Schubert, G., Spohn, T., 1990. Thermal history of Mars and the sulfur content of its core. J. Geophys. Res. 95, 14095–14104.
Schubert, G. et al., 1988. Mercury's thermal history and the generation of its magnetic field. Mercury, 429–460.
Schubert, G., Russell, C., Moore, W., 2000. Geophysics: Timing of the martian dynamo. Nature 408, 666–667.
Sekhar, P., King, S.D., 2014. 3D spherical models of martian mantle convection constrained by melting history. Earth Planet. Sci. Lett. 388, 27–37.
Sleep, N.H., 1994. Martian plate-tectonics. J. Geophys. Res. – Planets 99, 5639–5655.
Solomatov, V.S., Stevenson, D.J., 1993. Suspension in convective layers and style of differentiation of a terrestrial magma ocean. J. Geophys. Res. – Planets 98, 5375–5390.
Šrámek, O., Zhong, S., 2010. Long-wavelength stagnant lid convection with hemispheric variation in lithospheric thickness: Link between martian crustal dichotomy and Tharsis? J. Geophys. Res. 115, E09010.
Stadler, G. et al., 2010. The dynamics of plate tectonics and mantle flow: From local to global scales. Science 329, 1033–1038.
Stevenson, D.J., 2001. Mars' core and magnetism. Nature 412, 214–219.
Stewart, A.J. et al., 2007. Mars: A new core-crystallization regime. Science 316, 1323–1325.
Stixrude, L., Lithgow-Bertelloni, C., 2011. Thermodynamics of mantle minerals – II. Phase equilibria. Geophys. J. Int. 184, 1180–1213.
Tosi, N., Plesa, A.C., Breuer, D., 2013. Overturn and evolution of a crystallized magma ocean: A numerical parameter study for Mars. J. Geophys. Res. – Planets 118, 1512–1528.
Tuff, J., Wade, J., Wood, B.J., 2013. Volcanism on Mars controlled by early oxidation of the upper mantle. Nature 498, 342–345.
Turcotte, D., Schubert, G., 2002. Geodynamics. Cambridge Univ. Press, New York.
Van Thienen, P. et al., 2006. A top-down origin for martian mantle plumes. Icarus 185, 197–210.
Wanke, H., Dreibus, G., Wright, I.P., 1994. Chemistry and accretion history of Mars [and discussion]. Philos. Trans. R. Soc. A: Math., Phys. Eng. Sci. 349, 285–293.
Weiss, B.P. et al., 2002. Records of an ancient martian magnetic field in ALH84001. Earth Planet. Sci. Lett. 201, 449–463.
Wilhelms, D.E., Squyres, S.W., 1984. The martian hemispheric dichotomy may be due to a giant impact. Nature 309, 138–140.
Williams, J.-P., Nimmo, F., 2004. Thermal evolution of the martian core: Implications for an early dynamo. Geology 32, 97–100.
Zhong, S., 2009. Migration of Tharsis volcanism on Mars caused by differential rotation of the lithosphere. Nat. Geosci. 2, 19–23.
Zhong, S.J., Zuber, M.T., 2001. Degree-1 mantle convection and the crustal dichotomy on Mars. Earth Planet. Sci. Lett. 189, 75–84.